ISSN 0280-5316
ISRN LUTFD2/TFRT--5886--SE

Adaptive Control of Arm Movement based on Cerebellar Model

M. Mahdi Ghazaei A.

Department of Automatic Control
Lund University
June 2011

Lund University
Department of Automatic Control
Box 118
SE-221 00 Lund Sweden

Document name
MASTER THESIS

Date of issue
June 2011

Document Number
ISRN LUTFD/TFRT--5886--SE

Author(s)
M. Mahdi Ghazaei A.

Supervisor
Henrik Jörntell BMC Lund University, Sweden
Rolf Johansson Automatic Control, Lund Sweden (Examiner)

Sponsoring organization

Title and subtitle
Adaptive Control of Arm Movement based on Cerebellar Model. (Adaptiv styrning av armrörelser baserat på cerebellär model)

Abstract
This study is an attempt to take advantage of a *cerebellar model* to control a *biomimetic arm*. Aware that a variety of cerebellar models with different levels of details has been developed, we focused on a high-level model called MOSAIC. This model is thought to be able to describe the cerebellar functionality without getting into the details of the neural circuitry. To understand where this model exactly fits, we glanced over the biology of the cerebellum and a few alternative models.
Certainly, the arm control loop is composed of other components. We reviewed those elements with emphasis on modeling for our simulation. Among these models, the arm and the muscle system received the most attention. The musculoskeletal model tested independently and by means of optimization techniques, a human-like control of arm through muscle activations achieved. We have discussed how MOSAIC can solve a control problem and what drawbacks it has. Consequently, toward making a practical use of MOSAIC model, several ideas developed and tested. In this process, we borrowed concepts and methods from the control theory. Specifically, known schemes of adaptive control of a manipulator, linearization and approximation were utilized. Our final experiment dealt with a modified/adjusted MOSAIC model to adaptively control the arm. We call this model ORF-MOSAIC (**Organized by Receptive Fields** MOdular Selection And Identification for Control). With as few as 16 modules, we were able to control the arm in a workspace of 30 × 30 cm. The system was able to adapt to an external field as well as handling new objects despite delays. The discussion section suggests that there are similarities between microzones in the cerebellum and the modules of this new model.

Keywords

Classification system and/or index terms (if any)

Supplementary bibliographical information

ISSN and key title
0280-5316

ISBN

Language
English

Number of pages
78

Recipient's notes

Security classification

Degree Project in Robotics and Intelligent Systems
M. Mahdi Ghazaei A., June 29, 2011 (revised August 17, 2011)
mahdi.ghazaei.620@student.lu.se
Department of Automatic Control
Lund University, Faculty of Engineering (LTH)
www.lth.se

Acknowledgments

First of all, I would like to thank my “parents” that without their continuous support, I would not be able to take this challenging step in my life.

Thanks to **Professor Rolf Johansson**, I got acquainted to this amazing area of study. Furthermore, his presence and guidance during the project was a source of my inspiration. It was an honor to work under supervision of **Dr. Henrik Jörntell**. I would like to express my gratitude to him and his colleague **Dr. Fredrik Bengtsson** who patiently answered my ignorant questions in the field of neurobiology.

Not least, I wish to acknowledge the support of *Örebro University* during my leave.**Dr. Amy Lotfi**, the coordinator of *Robotics and Intelligent Systems* program helped me kindly through the procedure to do my thesis work remotely. I also thank **Dr. Dimitar Dimitrov** for helpful comments and discussions about this final report.

It was an enjoyable experience to work at a lively research environment in the Biomedical Center (BMC). Nonetheless, thanks to Anton Spanne and our fruitful discussions about different aspects of the computational models of the cerebellum, I felt totally at home.

Foreword

It is fascinating to see how living organisms evolve toward perfection despite the fact that the entropy of the universe constantly increases. It appears to me that for some particles, in this chaotic system with infinitely many feedback loops and adaptive parameters, there are fairly stable trajectories that drive them toward their destiny. I often wonder whether I should believe that this is an intrinsic property of the universe or rather I should look for a big plan and ultimately a designer!

Contents

1 Introduction **1**
- 1.1 Problem Formulation . . . 2
- 1.2 Methodology . . . 3
- 1.3 Organization of Thesis . . . 4

2 Biological Background of Cerebellum **5**

3 Computational Models **9**
- 3.1 MOSAIC . . . 9
- 3.2 Arm . . . 13
- 3.3 Muscle . . . 15
- 3.4 Sensory System and Lower Motor Control . . . 17
- 3.5 Trajectory Generation . . . 18

4 Experiments - Part 1 **21**
- 4.1 MOSAIC . . . 21
- 4.2 Arm with Muscles . . . 24

5 Toward a Complete Plant **25**
- 5.1 Additional Considerations . . . 25
- 5.2 Applicability of MOSAIC . . . 26
- 5.3 Possible Solutions . . . 27

6 Integrated Model **31**
- 6.1 Assumptions . . . 31
- 6.2 Implementation . . . 32
  - 6.2.1 Forward and Inverse Kinematics . . . 32
  - 6.2.2 Desired Trajectory . . . 33
  - 6.2.3 Minimum Tension Control . . . 34
  - 6.2.4 Adaptive Controller (Slotine) . . . 35
  - 6.2.5 FEL Controller . . . 36
  - 6.2.6 Improving Responsibility Signal . . . 37
  - 6.2.7 Receptive Fields . . . 39

7 Experiments - Part 2 **41**
- 7.1 Experimental Design . . . 41
- 7.2 Results . . . 44

8 Discussion **55**

9 Conclusion **59**

A Diagrams **67**

Chapter 1

Introduction

As robotic technology moves toward more anthropomorphic structures with increased complexity, it is reasonable to consider controllers inspired by human anatomy too. Although the robotics technology has achieved great performance in terms of accuracy, speed and robustness, the results are still quite limited to well-defined tasks. On the other hand, biological systems can operate under variety of conditions and their flexibility is yet unrivaled.

The study of control mechanisms in biological systems has attracted joint efforts of many roboticists and biologists. As a result, the first group will enjoy a richer set of design techniques incorporating some of the extraordinary capabilities of biological systems and the latter will find a new set of analysis tools which enables them to cast new light on our understanding of biological mechanisms.

One of the features of motor control in the vertebrates is fast-reaching movements in spite of long delays and noise in the nervous systems. It is believed that the cerebellum is mainly responsible to compensate for such deficiencies. Figure 1.1 presents the schematics of the motor control.

In the attempt to explain the functionality of the cerebellum, several computational models ranging from the cellular level to the functional level have been developed. The following list summarizes the major computational models [4, 46]:

1. Cerebellar Model Articulation Controller (CMAC)

2. Adjustable Pattern Generator (APG)

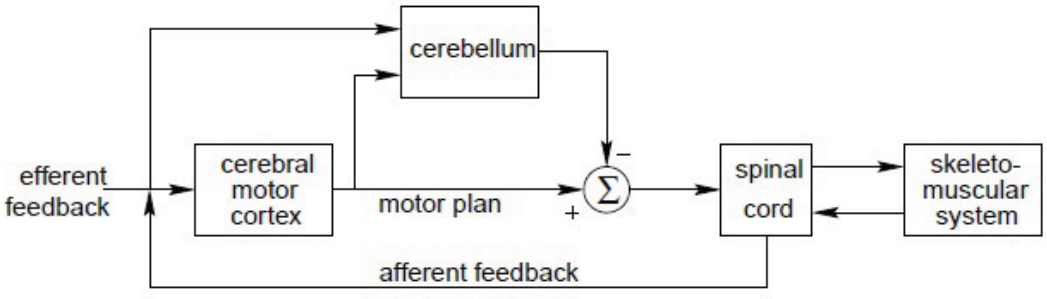

Figure 1.1: Simplified control loop relating cerebellum and cerebral motor cortex (taken from [77]).

3. Schweighofer-Arbib
4. Cerebellar feedback-error-learning model (CBFELM)
5. Multiple paired forward-inverse model (MPFIM)

Perhaps, CMAC is the earliest computational model proposed by Albus[2]. It is based on the idea of non-linear mapping between the command signals and the current state to the action (state encoder). However, the original work lacks the adaptation capability.

The APG model builds upon the observation that the cerebellar reverberating circuit and the inhibitory circuit of Purkinje cells can give rise to variety of resonating patterns [46]. It is named after its capability to generate elemental commands with adjustable intensity and duration [36]. The learning algorithm is able to adjust temporal patterns which are required for example in locomotion.

In Schweighofer-Arbib model [65], it has been striven to build more realistic models of the underlying neural cells in the cerebellar cortex. The model covers complete cerebellar circuitry including cells, axons, and fibers. However, several assumptions have been made due to the lack of biological data or simplification purpose.

The CBFELM starts from a functional level description and draws parallels with adaptive control schemes. In [49], vestibuloocular reflex (VOR) and the optokinetic eye movement response (OKR) based on this model have been studied. There are strong experimental evidences supporting the existence of an inverse model of the eye dynamics in the cerebellum and the feedback-error-learning [81].

The last model which was later on renamed to Modular Selection and Identification for Control (MOSAIC) [79, 32] shares the internal model principle with CBFELM. However, it additionally proposes a modular approach to provide high degree of flexibility without overly complicated control and adaptation mechanisms. Thereby, the key to success is an efficient way to combine these modules. The responsibility signals derived from the contextual information and the predictions of the forward models adjust the contributions of the paired inverse models encapsulated in each module.

1.1 Problem Formulation

In this research we aim to enhance robotic controllers in order to deal with more complex and less accurate embodiments thus improving their flexibility. This might be achieved by imitating the function of a part of CNS (Central Nervous System), viz. cerebellum, which is believed to play an important role by hosting an internal representation of the body dynamics.

In particular, we are interested to investigate the applicability of MOSAIC model as an auxiliary controller for a human-like robotic arm. The benefits and limitations of such architecture are to be studied. It is necessary to find out how effective the adaptive mechanism is and whether it could be made more robust to fulfill the requirements of an engineering application.

1.2 Methodology

This research clearly overlaps with several knowledge areas including biology, control theory, and computer science. Accordingly, it was necessary to look into the following subject areas.

- Biological structure and functions of the cerebellum
- Mechanical characteristics of human arm
- Multibody Simulation
- Theory of distributed adaptive control of nonlinear systems
- System identification and reinforcement learning

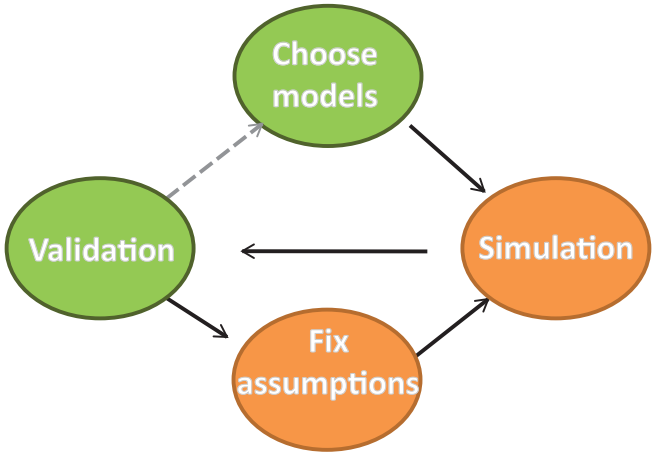

Figure 1.2: Work process, green ovals concerns mostly biology and orange ones control engineering

Ideally, we would like to use models which are as faithful as possible to the biology. However, because of the complexity of biological systems or ambiguities in our understanding of their functions, we had to occasionally deviate from this. In such cases, borrowing theories from control engineering or techniques form computer science was the solution. Specifically, MOSAIC as a model of the cerebellum is a high-level functional model which required adjustments for real applications.

All building blocks of an arm control loop were simulated by Matlab and/or Simulink. At each stage of simulation, we applied the required adjustments. Finally, in order to obtain an overall picture of the system performance, different test cases addressing convergence, stability issues, resilience to noise and delays, training and re-training attributes were devised.

While the main focus of this study was to build a reasonable adaptive control architecture for a simple model of human arm (in contrast to the verification of a cerebellum model), we considered a setup similar to [67] which makes comparison with the available experimental data possible.

1.3 Organization of Thesis

In Chapter 2,*Biological Background of Cerebellum*, a quick overview of the biological aspects of the cerebellum is presented. Chapter 3, *Computational Models* explains different components required to control arm movement from a computational perspective. Though these models form the basis of our simulations, we tried to provide sufficient explanation to give an idea to the reader about other alternatives. The rest of the thesis consists of two sets of problem and solution. In the first part of the experiments, Chapter 4, the result of modeling of the arm and the simulation of the MOSAIC model with a simple plant is presented. In Chapter 5, *Toward a Complete Plant* the results have been discussed and together with the next chapter, *Integrated Model* a way forward to integrate these two individual models has been suggested. Finally in Chapter 7, experiments with the complete plant is presented. We discuss about the remaining issues and future works in Chapter 8 and draw a conclusion in the final chapter.

Chapter 2

Biological Background of Cerebellum

The cerebellum is a region in the inferior posterior portion of the head. It occupies 10% of total brain volume and contains more than 50% of all neurons in the brain. It is part of a vast loop which receives nearly 200 million input fibers from cerebral cortex and brainstem areas and in return projects back to them. Many different inputs from spinal, vestibular, and trigeminal sources are integrated in the cerebellum that monitor the position and the motion of the body. Even visual and auditory signals are relayed via brainstem to the cerebellum which presumably provide additional sensory inputs that complement the proprioceptive informatiom [61]. In contrast to the cerebrum, the somatic sensory inputs are ipsilatterally mapped in the cerebellum at multiple sites (Figure 2.1).

The function of the cerebellum is mostly understood from pathologies and lesion studies. The most salient symptoms of cerebellar dysfunction are motor-related. The patients have difficulty producing smooth, well coordinated movements, instead, the movement tends to be jerky and imprecise. Depending on the damaged region, it causes loss of equilibrium, altered walking gait with wide stance, problems in skilled voluntary and planned movements. Some manifestations include tremors , dysmetria (problems judging distance or ranges of movement), dysdiadokinesia (inability to perform rapid alternating movements) which all together referred to as cerebellar ataxia.

The cerebellum is subdivided according to anatomy, phyologenetical features, and function to different areas. Structurally, it has three major components: laminated cerebellar cortex, a subcortical cluster of cells referred to as the deep cerebellar nuclei, and cerebellar peduncles which are large pathways to other part of the nervous system. From functional perspective, it consists of *vestibulocerebellum* regulating balance and eye movements, *spinocerebellum* regulating body and limb movement, and *cerebrocerebellum* involved in planning movement and evaluating sensory information for action [61].

The most distinctive cell body in the cerebellar cortex is called *Purkinje cell* (Figure 2.2). These are the solely outputs of the cerebellar cortex which inhibit the deep cerebellar nuclei. On the input side, they receive indirect inputs from mossy fibers through a layer of *granule cells*. Granule cells send T-shaped axons up to the Purkinje cells which form parallel fibers. A Purkinje cell receives excitatory inputs from several parallel fibers and an inhibitory input from a single

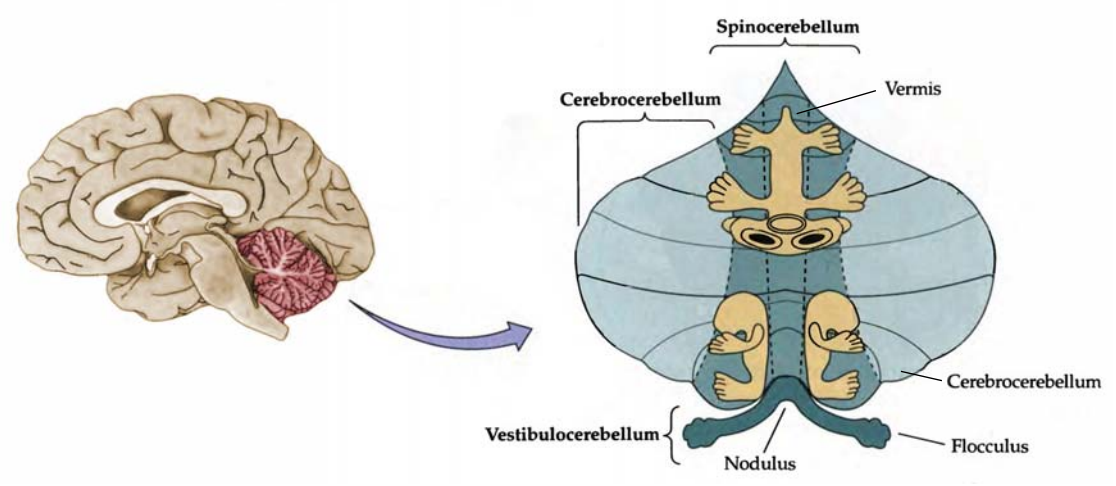

Figure 2.1: The cerebellum and a flattened view of the cerebellar surface illustrating the three major subdivisions and somatotopic maps of the body surface. The spinocerebellum contains at least two maps of the body. (modified from [61])

climbing fiber (CF). In addition to these inputs, two types of interneuron cells modulate the inhibitory activity of Purkinje cells. *Basket cells* make inhibitory complexes of synapses around Purkinje cell bodies and *stellate cell* receive input from parallel fibers and make inhibition to the Purkinje cell dendrites.

There is another type of cell called Golgi which make an inhibitory feedback loop around a granule cell. In other words it receives input from parallel fiber and inhibit the cell originating that fiber.

These cells are organized in three layers; from outer to inner, these are the molecular, Purkinje, and granular layers. The innermost layer contains the cell bodies of granule and Golgi cells. Mossy fibers enters this layer from pontine nuclei and send axons to the outermost layer viz. molecular layer. The human brain contains in the order of 60 to 80 million granule cells, making this cell type by far the most numerous in the brain. In the middle layer, there is only the cell body of Purkinje cells. Each Purkinje cell receive excitatory input from 100,000 to 200,000 parallel fibers. Finally the molecular layer contains, the two types of inhibitory interneurons, the parallel fiber tracks from Golgi cells and dendritic arbors of Purkinje neurons [1].

Neurons communicates through spikes. In case of Purkinje cells, there are two distinctive firing patterns - simple and complex spikes. A simple spike is a single action potential followed by a refractory period of 10 msec. "*complex spike*" is a burst of several spikes in a row, with diminishing amplitude, followed by a pause during which simple spikes are suppressed. In an awake behaving animal, the spike trains emit at mean rate of 50 Hz while the base line rate for climbing fiber activity is around 0.5-2.0 Hz [15].

The synapses between parallel fibers and Purkinje cells are susceptible to plasticity. The plasticity is induced either by Long Term Depression (LTD), decreasing the efficacy of synaptic connection or Long Term Potentiation (LTP) working inversely. The most plausible description has been given by the spike timing-dependent plasticity (STDP) model. The temporal interplay between a CF input (training signal), PC firing (postsynaptic factor), and PF synaptic ac-

tivity (presynaptic factor) produces brief electrical and chemical signals which lasts much longer [48].

The cerebellar cortex is divisible to saggital zones where each zone receives climbing fibers from a circumscribed area of the inferior olive and in return projects to specific deep cerebellar or vestibular nucleus. The zones can be further subdivided to microzones. A microzone is a narrow strip of cerebellar cortex within which all Purkinje cells receive climbing fiber inputs with a similar receptive field identity. It has also been shown that microzones can spread over several zones or different regions within a zone forming multizonal microcomplexes (MZMCs) [3].

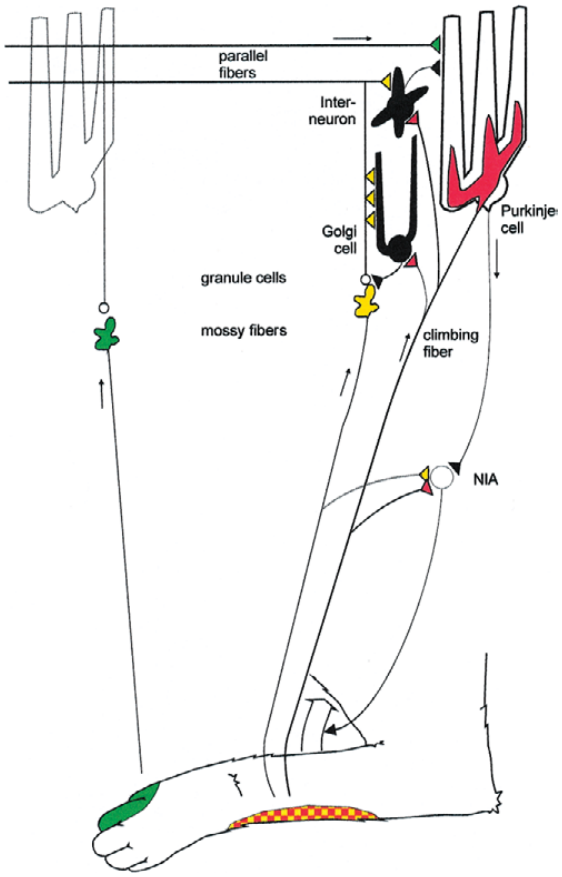

Figure 2.2: Schematic diagram of cerebellar neuronal circuit and its relationship to peripheral input and movement control. Green, peripheral receptive field for PF input to Purkinje cell. Red, peripheral receptive field for climbing fiber input, molecular layer interneuron and Golgi cell. Yellow, peripheral receptive field of PF input to interneuron and Golgi cell as as inhibitory receptive field of Purkinje cell. The bent arrow, indicates the movement controlled by the Purkinje cell via nucleus interpositus anterior (NIA) (courtesy of H. Jörntell [17]).

Chapter 3

Computational Models

In this chapter, we review MOSAIC as a model of the cerebellum in more details. Additionally, other models essential to the arm control are introduced.

3.1 MOSAIC

MOSAIC is a high level functional model inspired by the cerebellum. It aims to describe different behavioral observations such as context dependent control or generalization to new tasks. There are a few fundamental assumptions in this model. Most importantly, it advocates the internal model hypothesis which states that the cerebellum realizes an internal model of the body parts in order to successfully control them [80, 27]. This is in sharp contrast with the Equilibrium Point Hypothesis (EPH) which only requires that the Central Nervous System (CNS) defines the end-point muscle tensions. The EPH is motivated by the fact that for any set of springs pulling across multiple joints, there is a stable position into which the limb could passively settle [66].

However, it has been argued against the usefulness of equilibrium point motion (i.e., by following the time series defined by succession of such equilibrium points called a virtual trajectory). The main objection is due to the complexity of the required virtual trajectories under low stiffness and fast movement of the arm [44]. Moreover, by measuring actual stiffness of the joints during movement, it has been shown that the predicted trajectory by the EPH differs substantially from the real one [27]. Therefore, the internal model seems more tenable than the EP hypothesis.

Internal models come in two different flavors. A forward model indicates the causal direction from motor commands into their sensory consequences, whereas an inverse model indicates the relation between the desired state and the required input to achieve this. For example, the (Vestibulo-ocular reflex) VOR control system must compute the motor command that is predicted to yield a particular eye velocity to compensate for head movement. Accordingly, a major aspect of motor learning can be stated as the acquisition of forward and inverse internal models.

According to Figure 3.1, the structure of MOSAIC hosts both forward models and inverse models paired in modules. Modularity is thought to be another important feature of the motor control [55], in particular cerebellum [21, 22].

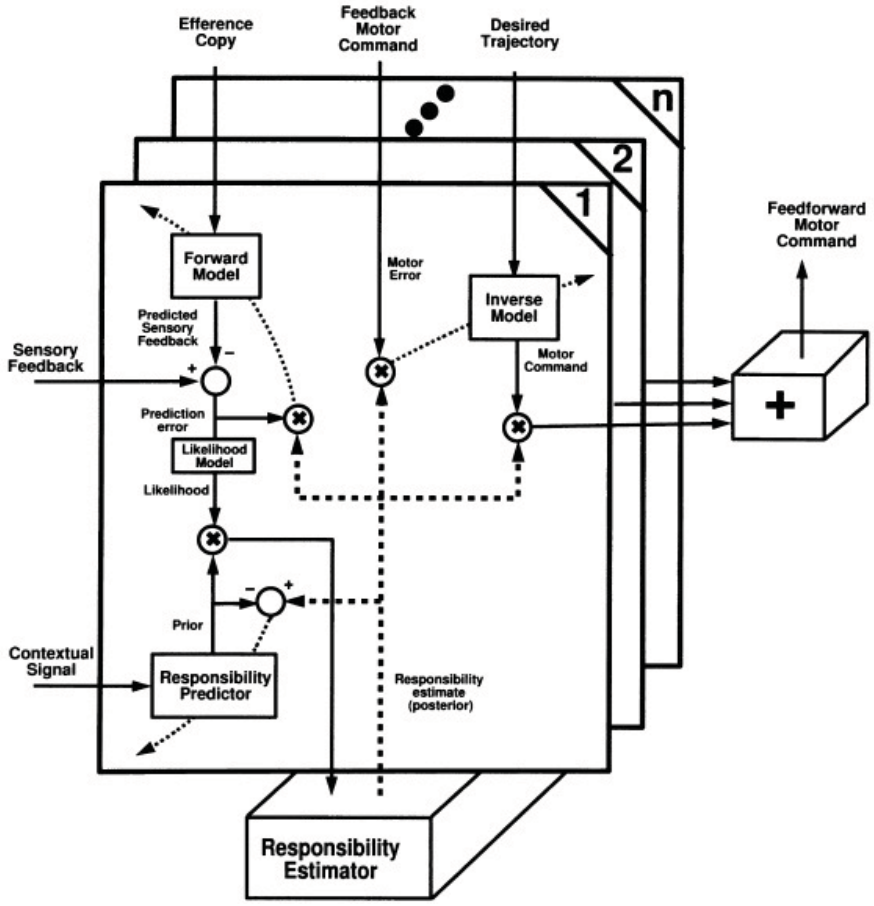

Figure 3.1: A schematic of the MOSAIC model (taken from [79])

The forward models which have access to the sensory feedback and the efference copy[1] predict the current context. Each module gets a portion of the responsibility in controlling a plant based on the quality of the prediction of its forward model. The forward models and inverse models could be mathematically formulated as:

$$\hat{\mathbf{x}}^i_{t+1} = \phi\left(\mathbf{w}^i_t, \mathbf{x}_t, \mathbf{u}_t\right) \tag{3.1}$$

$$\mathbf{u}^i_t = \psi\left(\mathbf{v}^i_t, \mathbf{x}^*_{t+1}, \mathbf{x}_t\right) \tag{3.2}$$

$$\mathbf{u}_t = \sum_{i=1}^{n} \lambda^i_t \mathbf{u}^i_t \tag{3.3}$$

where $\mathbf{x}^*$, $\mathbf{x}$, and $\hat{\mathbf{x}}^i$ are the desired state, the sensory feedback, and the output of i-th forward model respectively. Here, $\mathbf{u}^i_t$ represents i-th module's control signal, $\mathbf{u}_t$ the total control signal. The inverse and forward functions are $\psi()$ and $\phi()$ respectively. The vector of the parameters are represented by $\mathbf{w}^i_t$ and $\mathbf{v}^i_t$.

It must be noted here that, this usage of the forward models is different than the standard internal model control (IMC) in schemes such as Smith predictor.

[1] A motor signal from the CNS to the periphery is called an efference, and an internal copy of this signal is called an efference copy. Among others, an efference copy enables the brain to predict the sensory feedback from movements and to distinguish between self-generated and exogenous signals.

In IMC based design, a controller acts upon the new information existing in the difference between the output of the real system and its internal forward model [24] whereas in MOSIAC the main purpose of the forward models is partitioning the state space. In that respect, MOSAIC is conceptually similar to the mixture of experts [26, 42]. In addition, an inverse model could be built by using a recurrent structure which is proposed in the decorrelation controller interpretation of the cerebellum [13, 60].

For training such networks, two questions must be confronted; which module and when it must be trained. These are formally known as *structural* and *temporal credit assignment*. The *responsibility signal* plays an important roll in both structural and temporal credit assignment since it adjusts the learning rate for forward models and inverse models.

Assuming a Gaussian posterior probability and a prior probability as a function of the current context y_t and a parameter vector δ_t^i, the responsibility signal is defined as

$$P_t^i = \eta\left(\delta_t^i, y_t\right) \tag{3.4}$$

$$p\left(x_t|w_t^i, u_t, i\right) = \frac{1}{\sqrt{2\pi\sigma^2}} e^{-\left|x_t - \hat{x}_t^i\right|^2/2\sigma^2} \tag{3.5}$$

$$\lambda_t^i = \frac{P_t^i p\left(x_t|w_t^i, u_t, i\right)}{\sum_{j=1}^n P_t^j p\left(x_t|w_t^j, u_t, j\right)} \tag{3.6}$$

where σ is a parameter that tunes the sensitivity to the prediction error of a forward model.

Accordingly, the following update rule applies to the forward model:

$$\Delta w_t^i = \epsilon \lambda_t^i \frac{d\phi_i}{dw_t^i}\left(x_t - \hat{x}_t^i\right), \tag{3.7}$$

where ϵ is the learning rate.

In general, inverse model learning is possible by *a*) direct modeling: e.g. through motor babbling and observing input and output data. This approach runs into difficulty in case of extra degrees-of-freedom; *b*) feedback-error-learning (FEL): the feedback controller transforms the trajectory error in sensory coordinates, into a feedback motor command; or *c*) distal supervised learning: a froward model is used to convert outcome errors into the errors in the motor command [43].

Distal error problem for supervised learning is present whenever the standard of correctness is available in a coordinate systems that is different from the one in which the learning system produces its output. Reinforcement learning can offer another approach to solve this problem since it does not require error vectors.

The following equation represents the update rule of the inverse models. This is FEL where the feedback error, u_{fb}, approximates the actual error in the command coordinate.

$$\Delta v_t^i = \epsilon \lambda_t^i \frac{d\psi_i}{dv_t^i}\left(u_t^* - u_t^i\right) \simeq \epsilon \lambda_t^i \frac{d\psi_i}{dv_t^i} u_{fb} \tag{3.8}$$

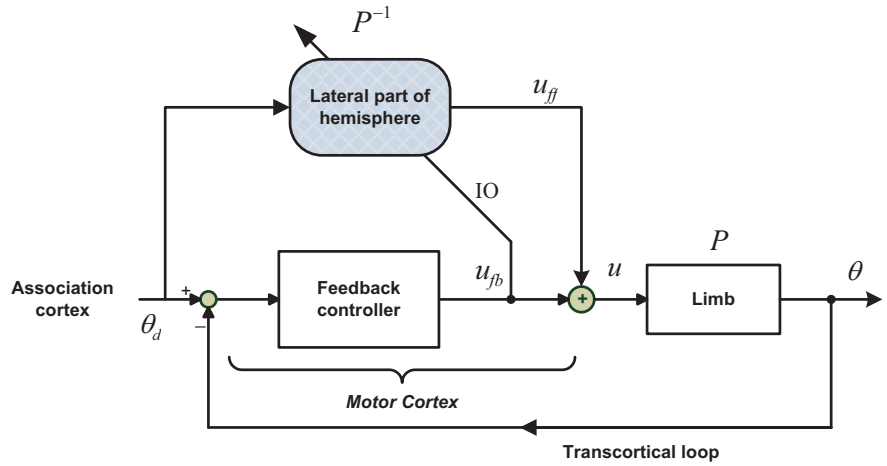

Figure 3.2: Block diagram for voluntary-movement learning control by a corticonuclear microcomplex in a cerebro-cerebellar communication loop (adapted from [50]).

Ito has viewed the cerebellum as an adaptive side path to the descending system, modulating the feedforward commands issued by cerebral control centers. While Kawato considers it as an alternative to these cerebral systems, replacing their control function [53]. Both inverse model controllers and FEL fit quite well in the Kawato's view of the cerebellum [50, 45] and hence MOSAIC.

In fact, gradient descent update rules reminds of Fujita's heterosynaptic plasticity rule [20]. This single rule can reproduce the effect of both LTD and LTP for the synaptic efficacy of a single parallel fiber synapse [46].

$$\tau dw_i/dt = -x_i \left(F - F_{spont}\right), \tag{3.9}$$

where τ is the time constant, w_i is the synaptic weight of the ith parallel fiber-Purkinje cell synapse, x_i is the firing frequency of the ith parallel fiber-Purkinje cell synapse, F is the firing frequency of the climbing fiber input, and F_{spont} is its spontaneous level.

Since the original paper on MOSAIC [79], there have been some development in its application and a few extensions. There is a successful report on the application of the original proposal for controlling three different objects, characterized by different mass, weight, and damping factor. In this report, the system was able to learn multiple tasks(controlling an object), generalize to a new task and switch between tasks appropriately [30].

HMM-MOSAIC [32], is a variant which make use of Hidden Markov Model (HMM) for improving both the training and the switching aspects of MOSAIC. The methodology is inspired by speech processing techniques and the training algorithm is a specialized instance of Expectation Maximization (EM) algorithm. Though it is difficult to motivate this probabilistic approach biologically, it is argued by the authors that the context estimation by human could be well described by HMM models.

The same authors extended their model later to a hierarchical MOSAIC, ***HMOSAIC*** [31]. In this paradigm, the modules could be cascaded. A higher-level MOSAIC receives an abstract desired trajectory and posterior probabilities

of its subordinate level and generates as a motor command, prior probabilities for the lower-level modules. The model was tested with the same three objects.

In [73], ***e-MOSAIC*** has been proposed and used for humanoid robot control. In this architecture, forward models serve as state estimators in form of Kalman filters and contribute to the overall state estimate. Instead of inverse models, for each observer a matching Linear Quadratic (LQ) controller is designed which together with the overall state estimate, functions as a (Linear Quadratic Gaussian) LQG controller. The responsibility weighted summation of these LQG controllers constitute the control signal. The models are fixed with no adaptation.

MOSAIC scheme has also been extended to the reinforcement learning paradigm as ***multiple model-based reinforcement learning (MMRL)***, in which each inverse model controller was replaced by a reinforcement learning agent [14]. The authors have developed discrete and continuous cases in parallel and tested the structure in a haunting task in a grid world and for controlling an inverted pendulum.

In order to control sit-to-stand task, an automatic module assigning MOSAIC, ***AMA-MOSAICI*** has been proposed [18]. The whole task is decomposed to linear subtasks by a clustering algorithm. The main feature of this work is that the number of the required modules is automatically determined. However, both clustering and training are done off-line.

3.2 Arm

The dynamics of a human arm could be analyzed similarly to solid multi-joint manipulators. The equations of motion are usually derived by the Lagrange's equations. These equations have a generic form of:

$$\mathbf{H}(\boldsymbol{\theta})\ddot{\boldsymbol{\theta}} + \mathbf{C}(\boldsymbol{\theta}, \dot{\boldsymbol{\theta}}) + \mathbf{G}(\boldsymbol{\theta}) = \boldsymbol{\tau} \tag{3.10}$$

where $\mathbf{H}(\boldsymbol{\theta})$ is a symmetric positive definite inertia matrix, $\mathbf{C}(\boldsymbol{\theta}, \dot{\boldsymbol{\theta}})$ is the vector of centripetal and Coriolis torques, and $\mathbf{G}(\boldsymbol{\theta})$ is the term due to gravity. $\boldsymbol{\theta} \in \mathbb{R}^n$ is the vector of joint angels and its time derivatives denoted by dot operator. The system is driven by torque vector, $\boldsymbol{\tau} \in \mathbb{R}^n$.

It is known that a human arm has 7 degrees of freedom (DOF) in its kinematic structure while 6 DOF are sufficient for manipulating objects [8]. For the sake of simplicity, a two link model can represent the human arm. If we further limit the motion in a horizontal plane, only two joints with one degree of freedom are required and the effect of the gravity is ignored. In case of two links without excluding the gravity, the matrices in Equation 3.10 are as follows:

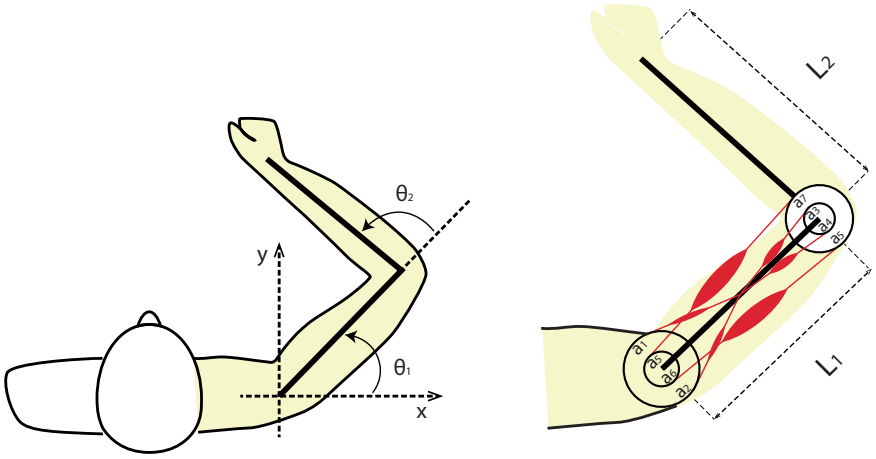

Figure 3.3: Schematic of Arm and its geometry

$$\mathbf{H} = \begin{bmatrix} h_{11} & h_{12} \\ h_{12} & h_{22} \end{bmatrix} \tag{3.11}$$

$$\begin{aligned} h_{11} =& m_2 L_1^2 + m_1 r_1^2 + I_1 + 2 m_2 r_2 L_1 \cos(\theta_2) + m_2 r_2^2 + I_2 \\ h_{12} =& m_2 r_2 L_1 \cos(\theta_2) + m_2 r_2^2 + I_2 \\ h_{22} =& m_2 r_2^2 + I_2 \end{aligned}$$

$$\mathbf{C} = \begin{bmatrix} -2 m_2 r_2 L_1 \dot{\theta_1} \dot{\theta_2} \sin(\theta_2) - L_1 m_2 \dot{\theta_2}^2 r_2 \sin(\theta_2) \\ m_2 r_2 \dot{\theta_1}^2 L_1 \sin(\theta_2) \end{bmatrix} \tag{3.12}$$

$$\mathbf{G} = \begin{bmatrix} m_2 r_2 g \cos(\theta_1 + \theta_2) + m_2 L_1 g \cos(\theta_1) + m_1 r_1 g \cos(\theta_1) \\ m_2 r_2 g \cos(\theta_1 + \theta_2) \end{bmatrix}, \tag{3.13}$$

where the subscripts of θ indicate its elements; the gravitational acceleration is denoted by g; with indices denoting the link number, m, l, r, and , I refer to link mass, link length, the distance between the previous joint to the center of the gravity of a link, and moment of inertia around the center of mass respectively. These values for an average male person could be chosen according to Table 3.1 [33].

Table 3.1: Geometrical and dynamical parameters of the arm

	m (kg)	L (m)	r (m)	I (kg.m^2)
Link 1	1.59	0.3	0.13	0.0216
Link 2	1.44	0.35	0.14	0.0089

Another aspect of a human arm is its musculo-skeletal structure. In other words, how muscles are connected to the bones. In reality, major prime movers are extended over more than one joint [28]. However, with an eye on robotic application, a model according to Figure 3.3 could be used. This model has the feature of both *mono-articular* and *bi-articular* muscles and with right parameters can closely simulate a human arm [44].

The relation between muscles and an arm can generally be written as

$$\tau(\theta, \dot{\theta}, u) = - A(\theta)^T T(\ell, \dot{\ell}, u) \tag{3.14}$$
$$\ell = L(\theta). \tag{3.15}$$

Here $l \in \mathbb{R}^m$ and θ are the actual muscle length and joint angle vectors; τ is the joint torque generated by agonist and antagonist muscles; $T \in \mathbb{R}^m$ is the muscle tension vector; $A(\theta) \in \mathbb{R}^{2\times m}$ is the moment arm matrix; $u \in \mathbb{R}^m$ is the motor command vector fed to the muscles where m is the number of muscles. The muscle lengths are uniquely determined from the joint angles by function $L(\theta)$.

By assuming constant moment arm matrix which do not depend on joint angles, $A(\theta) = A$, the muscle vector is given as

$$\ell = \ell_m - A\theta \tag{3.16}$$
$$A = \begin{pmatrix} a_1 & a_2 & 0 & 0 & a_5 & a_6 \\ 0 & 0 & a_3 & a_4 & a_7 & a_8 \end{pmatrix}^T, \tag{3.17}$$

where l_m is the muscle length when the joint angle is zero.

Table 3.2 represents the average of anatomical data for matrix A [44].

Table 3.2: a_1, shoulder flexor; a_2 shoulder extensor; a_3 elbow flexor;a_4 elbow extensor; a_5 and a_6 double-joint flexor; a_6 and a_7 double-joint extensor;

	a_1, a_2	a_3, a_4	a_5, a_6	a_6, a_7
Moment arm (cm)	4.0	2.5	2.8	3.5

3.3 Muscle

A muscle is composed of many long, thin cells, called fibers arranged in parallel. The fibers are composed of several thousand myofibrils which, in turn, composed of microscopic units called sarcomeres. Sarcomers are the basic contractile units of muscles. Muscle contractile properties depend on the fiber length and muscle cross-sectional area. Therefore, they are usually normalized by these parameters [51]. The rate of change in the length of a muscle have a non-linear relation to the force it can exert.

Muscle models could be categorized in three major groups based on their complexity:

1. input-output models: they are often in form of linear transfer functions from neural excitation to force. Second order models are the most common.

2. lumped parameter mechanical models: These models composed of different mechanical elements such as springs and dashpots to represent viscoelastic property of a muscle. It is also possible to incorporate non-linear force-velocity behavior of a muscle or tendon properties into them. These

models are named after A.V Hill as Hill models [34]. The benefit of Hill-type models is that they have directly measurable mechanical properties. Model inputs may be neural excitation, or length and force perturbations, and outputs can include stiffness, and the time course of muscle length changes besides muscle force. These models are even called by their corresponding mechanical model names, known as the standard solid model or simpler ones, Kelvin-Voigt containing only a parallel spring damper or Maxwell model containing a spring in series with a damper [59].

3. cross-bridge models: They try to capture the dynamics of molecular process that is responsible for force generation. A cross-bridge is a population of molecular projections between two sets of interdigitating protein filaments building up a sarcomer and can produce a ratchet-like action. Inputs in these models can consist of neural excitation pulses or mechanical perturbations,while outputs can cover a wide range of mechanical variables and thermodynamic information.

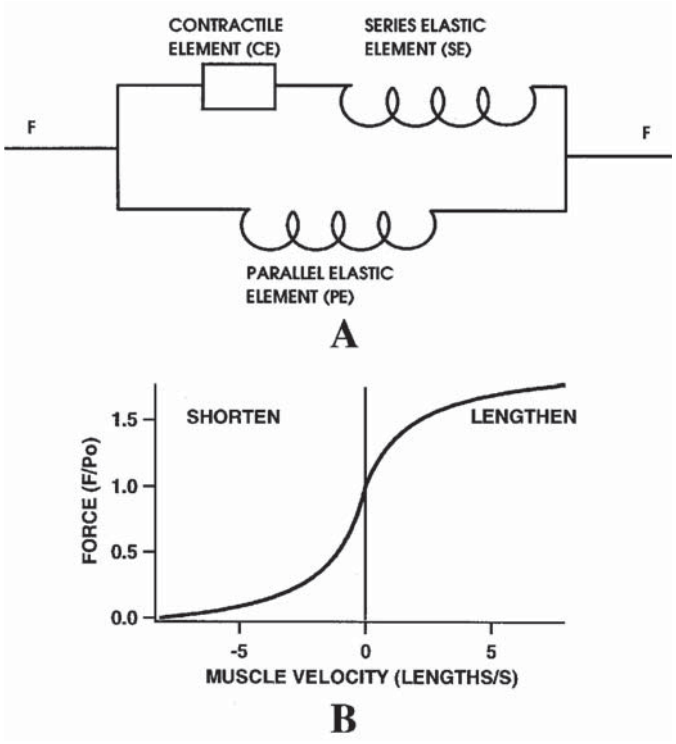

Figure 3.4: Schematic of (A) Hill model structure, (B) the force-velocity relation for both concentric and eccentric regions (taken from [51]).

Among the above mentioned models, Hill-type models are by far the most widely used. However, they cannot predict "yield" and has no mechanism to handle varying cross-bridge persistence observed with different movement histories.

Many other factors seem to be important in modeling. For instance, though the tendon is usually modeled as an ideal spring they have more complex properties. The energy storage property of it, plays an integral role in efficient jumping locomotion. For correct understanding of muscle function, it is also nec-

essary to understand the process that engages muscle fibers, i.e. motorneuron recruitment.

On the other hand, the complex structure of muscle system seems to offer some benefits. For example, muscle stiffness increases approximately linearly with muscle activation [58].

Ignoring the series elastic element in Figure 3.4 (A) results in Kelvin-Voight model. In this model, the muscle tension, T, is determined by

$$T(l, \dot{l}, u) = K(u)\,(l_r(u) - l) - B(u)\dot{l} \tag{3.18}$$

where l is the muscle length vector, $\dot{l}$ is the contraction velocity vector and $l_r(u)$ the rest length of the muscle. $K(u)$ and $B(u)$ denote muscle stiffness ad viscosity respectively. In general all these parameters depend on the motor neuronal activations u, however following [44] for simplicity we assumed that they are linear functions of the motor command u:

$$K(u) = k_0 + ku \tag{3.19}$$
$$B(u) = b_0 + bu \tag{3.20}$$
$$l_r(u) = l_0 + ru \tag{3.21}$$

Here k_0, b_0 and l_0 are intrinsic elasticity, viscosity and rest length when u is zero. In our simulations, we used the same parameter values as [44].

3.4 Sensory System and Lower Motor Control

There are two main sources of feedback directly from limbs. Cutaneous inputs from the skin area is believed to provide kinesthetic information [6]. Moreover, it is shown that joint parameters could be sufficiently encoded by the skin receptors [5].

Muscles are also equipped with the so called proprioceptors. The afferent from these elements provide feedback about the state of the arm and its movements. Muscle spindles are attached in parallel to the extrafusal fibers which are responsible for the actual movement. The spindles are fine intrafusal muscle fibers containing a fluid-filled capsule and give rise to the primary afferent, Ia, and the secondary afferent, II. Roughly speaking, Ia signals the rate of change in muscle length while type II afferents are correlated with the length of muscles [37].

Type I and II are differentiated because of the thickness of the fibers and hence their transmission speed. Furthermore, Gamma motor neurons contracts the spindle affecting its discharge rate. Muscles contract following the excitation by alpha motor neurons. By coactivation of α-γ, The neural mechanism makes it possible to detect external perturbations in order to compensate for them. The FLETE model affording independent control of muscle's lengths and tensions provides a good picture of the mechanism of this part of the spinal circuitry [7].

In addition to the muscle spindles, there are Golgi tendon organs (GTO) located between extrafusal muscle fibers and tendons and give rise to Ib afferents.

GTO's discharge rate increases by the increase in the tension in muscle and decreases as it is released [68].

The neural reflex circuit makes use of the spindle and the GTO so that the change in length and tension is automatically opposed. The circuitry and a schematic of this mechanism is shown in Figure 3.5.

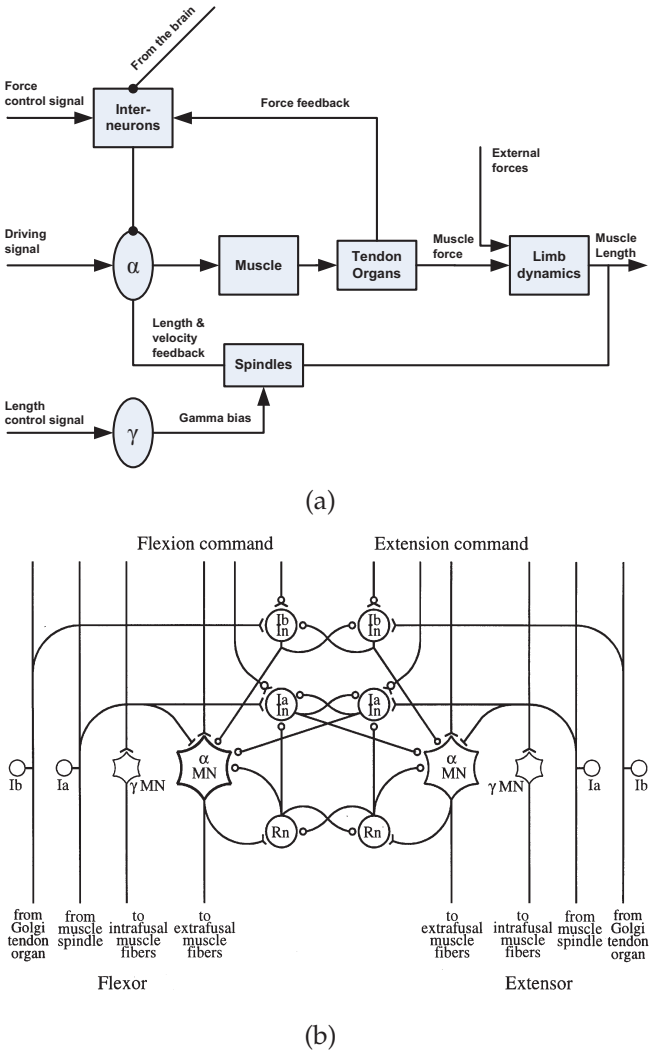

Figure 3.5: Sensory feedbacks and spinal reflex mechanism: (a) schematic diagram of reflex and descending pathways, arrows show excitatory inputs and circles inhibitory connections, (modified from [68]); (b) Neural reflex circuitry of the spinal segment, the abbreviations are (MN) motorneuron, (IaIn) Ia inhibitory and (IbIn) Ib inhibitory interneuron, (Rn) Renshaw cell. Line segments and open circles represent excitatory and inhibitory synapses respectively (taken from [9]).

3.5 Trajectory Generation

The simplest kinematic description of the trajectory is given by *minimum jerk model* [19]. It is meant to predict the bell shaped velocity profile of arm movement. In a planer case, the optimization criterion is as follows:

$$C = \frac{1}{2} \int_0^{t_f} \left(\left(\frac{d^3x}{dt^3} \right)^2 + \left(\frac{d^3y}{dt^3} \right)^2 \right) dt, \tag{3.22}$$

where x and y represent the coordinate and t_f the duration of the movement.

Another descriptive model is the $2/3$ law which relates the geometry of movement to the velocity. The $2/3$ law states that the angular velocity is related to the curvature of the trajectory path by a power law and a proportionality constant. A variation of minimum jerk model called *constrained minimum jerk model* [74] optimizes jerk too but under the constraint of a predefined path. Therefore, it is not limited to the via-points for more complex paths and similar results to the $2/3$ law could be derived.

There are models trying to find the underlying principles of the movements. Among them, minimum torque-change and minimum motor-command-change are meant to minimize "wear and tear" in the actuators [8].

There is another view that holds the neural level and the goal of accurate reaching responsible for the observed trajectories [29]. In contrast to the previous methods which try to maximize smoothness or efficiency, the precision is maximized in this approach. With a more generic application, it is named TOPS (Task Optimization in the Presence of Signal Dependent Noise) [8].

Chapter 4

Experiments - Part 1

4.1 MOSAIC

In this experiment, mainly the work done in [30] has been replicated. The main difference is that we have used minimum jerk trajectory instead of Ornstein-Uhlenbeck(OU) process [75]. Since OU process is a random process, it has a better excitation characteristic. However, minimum jerk trajectory turned out to be sufficient. The objects are switched cyclically every 10 seconds between the three objects shown in Figure 4.1.

Figure 4.2 shows that after adaptation, the forward modules correctly select the inverse controllers and the control is done in a feedforward manner (negligible feedback signal).

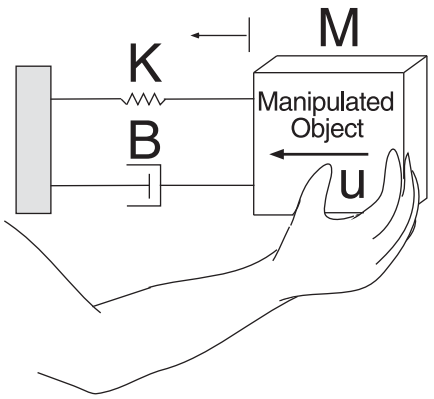

	M(Kg)	B(Ns/m)	K
α	1.0	2.0	8.0
β	5.0	7.0	4.0
γ	8.0	3.0	1.0

Figure 4.1: Schematic illustration showing the properties of three manipulated objects with mass M, damping B, and spring factor K (adapted from [79]).

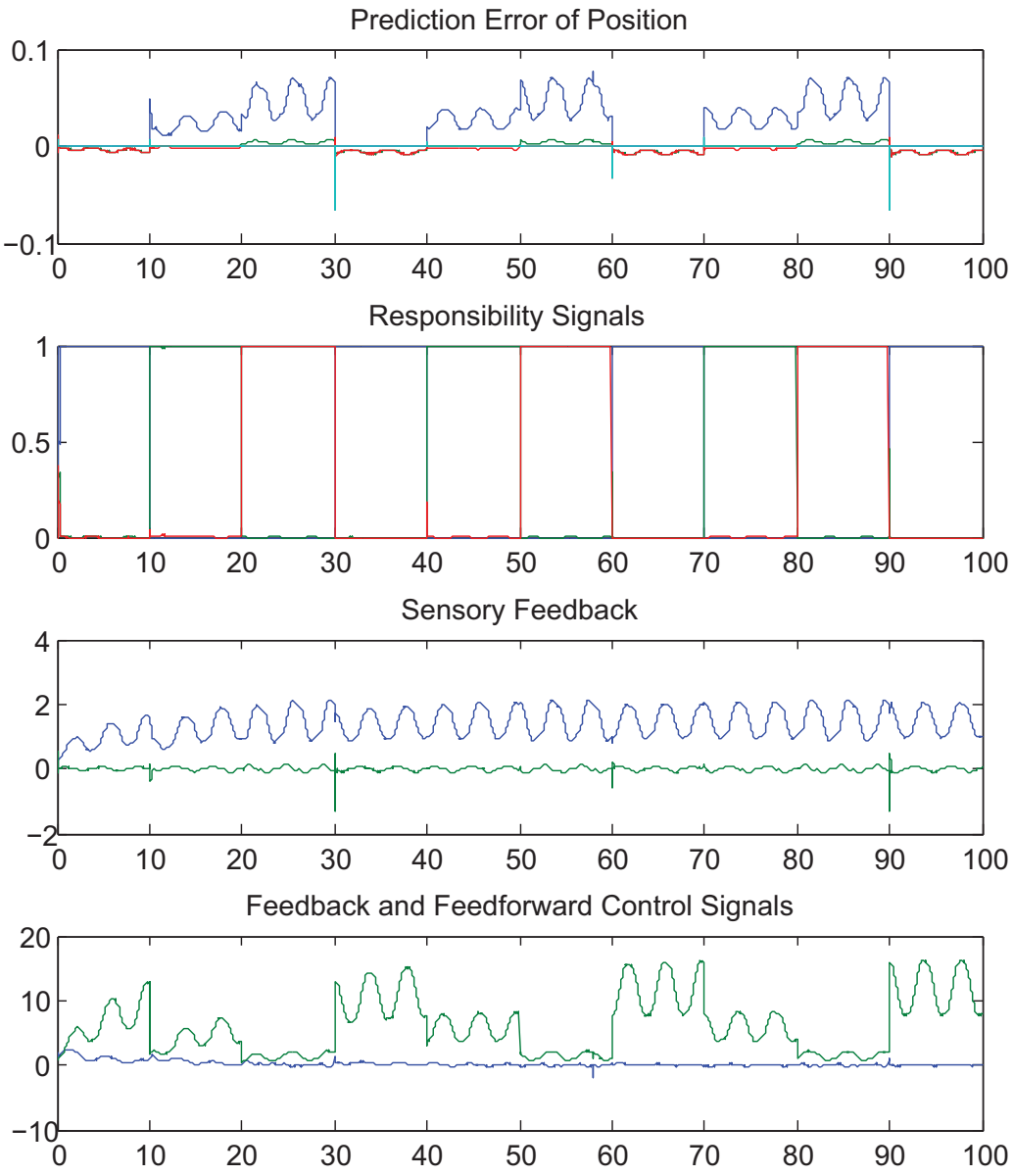

Figure 4.2: Simulation of MOSAIC while switching between three objects, blue object one, red object two, and green object three. The horizontal axis shows time in seconds.

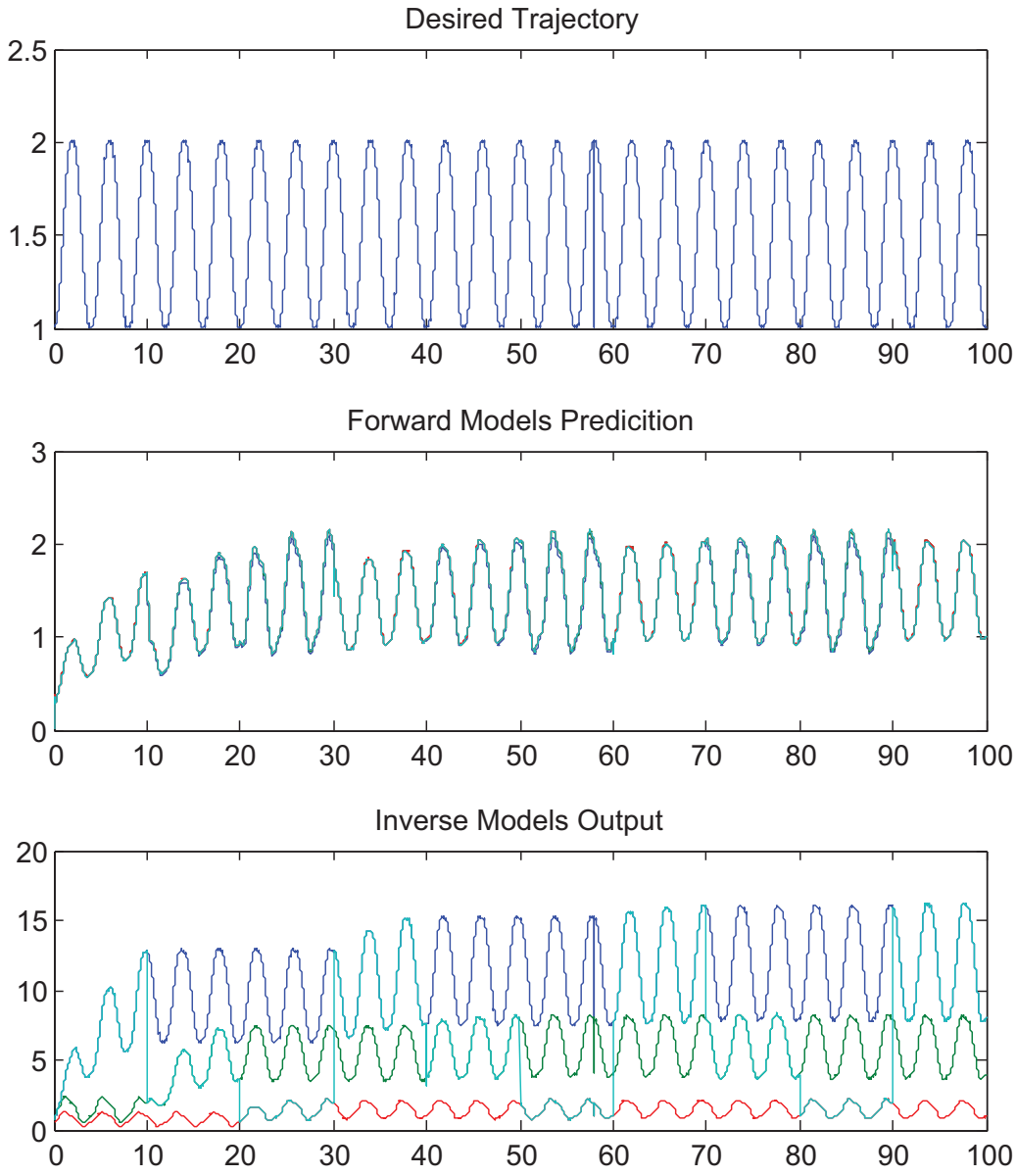

Figure 4.3: Simulation of MOSAIC while switching between three objects, blue object one, red object two, and green object three, cyan overall estimate or overall output. The horizontal axis shows time in seconds.

4.2 Arm with Muscles

In this experiment the musculoskeletal model of the arm according to Sections 3.2 and 3.3 has been tested. Figure 4.4 shows the movement of the arm with constant muscle activation. Because of the viscoelastic property of the muscles, it is observed that the arm oscillates before it settles down in the final position.

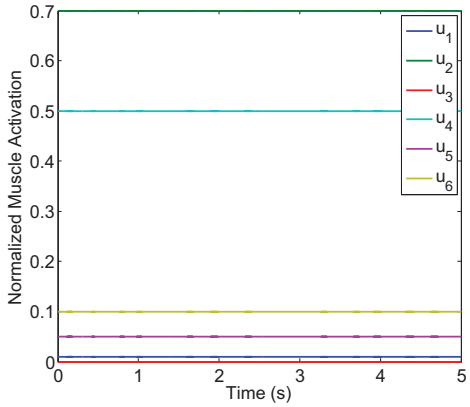

(a) Muscle activations

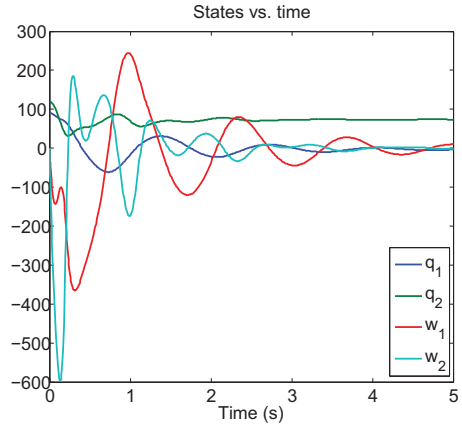

(b) Joint angles (deg) and joint angular velocities (deg/s)

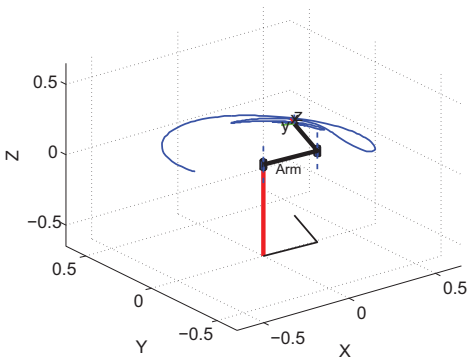

(c) Hand trajectory and final arm position

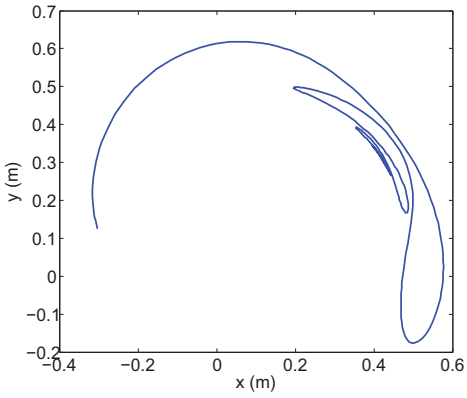

(d) Hand trajectory

Figure 4.4: Movement of arm with constant muscle activation.

Chapter 5

Toward a Complete Plant

There have been many attempts to simulate the motor control loop for the arm [71, 65, 72, 56, 38]. Such works vary in the details of the models and the assumptions. Among others, [10] because of the level of detail and the attempt to be faithful to the biology is notable. In Chapter 3, we discussed about different components which are required to build a complete plant. Here, we discuss mainly about the potential problems with MOSAIC and remaining elements which make an end-2-end simulation possible.

5.1 Additional Considerations

The main components of the control loop of the arm were reviewed in Chapter 3. However, important questions still need to be answered.

In what coordinate system the signals in the brain are represented? At least four coordinate systems are distinguishable: task space where tasks are defined possibly in terms of sensor reading , workspace corresponding to six-dimensional Cartesian space, joint space determining configuration of joints, and actuator space where actual motion commands are issued. There are evidences for joint-based control [67]. However, this implies transformation from joint to actuator space (muscle space). It is not totally clear what the neural substrate of such transformations is. The transformation between torques to muscle tensions, has been suggested to happen in C3/C4 network [64]. Given a simple model for the muscles, they have implemented an ideal joint to actuator space transformation by algebraic equations.

The control system in human is highly hierarchical. How important lower level motor control such as stretch reflex is? Does higher level motor control take advantage of muscle synergy in the spinal motor circuits to simplify the motor control [12]?

Motor learning does not happen at once and usually undergoes a period of consolidation. The central nervous system has specific strategies for learning which are sometimes related to the stage of development. In addition, it is strongly argued against rote learning of a trajectory. With regard to different tasks, we need to find out how we store and recall learned plans.

5.2 Applicability of MOSAIC

During the experiments with the original MOSAIC model, it was made clear that even our simplified model of the arm seems to be too complex to be controlled by it. These observations are summarized in the following list:

1. MOSAIC does not efficiently distribute responsibilities between modules: In other words, there is no guarantee that each module takes a portion of the responsibility. Thus, it is possible that only one module gets adapted and controls while the rest are unused or all do the same thing.

2. The responsibility signal is based on one sample prediction and therefore not reliable: It might cause chattering where switching back and forth between two controllers happens

3. Combination of models does not constitute stable equilibrium points in relation to the adaptation: As it is expected from MOSAIC, new functions should be attained by combining the previously learned modules. Even if the responsibility predictors correctly combine the controllers, small errors would force one system to specialize if it is possible.

4. Performance is limited by the quality of the forward models: The quality of responsibility signals and the value of sigma parameter in Equation 3.5 have a critical effect on the performance of the model.

Besides the above mentioned issues, there are undefined elements by the structure of MOSAIC. Most importantly, how inverse and forward models should be chosen and implemented. One alternative would be an exact replication of biological circuits (at least for the control part of the modules where it is possible). The main drawback of this approach is that the stability criteria is difficult to be evaluated and the training procedure is not clear. This is partly due to our lack of comprehensive knowledge about the nature of biological signals.

It is right to question why different modules are required in the first place [55]. In a very abstract way, modules can break a complex systems into simpler and more manageable ones i.e. they are easier to be designed, trained, etc. The easiest way would be to consider a partitioning principle such as different domains in time, space, frequency, etc. From a more cognitive perspective which seems to be the motivation for such models, we can divide up an experience according to specialized tasks (e.g. manipulating different objects) or for different subtasks (e.g. part of the trajectory in sit-to-stand movement). These give rise to the notion of *functional modules* vs. *state based modules*. By state based modules, we mean modules corresponding to different operating point thus excluding internal parameters of a system from the state definition.

Another question is what role plasticity plays. It could be conjectured that it is the substrate of the adaptive mechanism required for the existing internal models to cope with small changes in the plant. It could also be seen as a way to acquire new skills. It is questionable how it might affect the already trained modules in relation to new tasks.

In this generic view of the modules, a trade-off between unit complexity vs. the number of the modules is imaginable. In other words, one can reduce the

number of modules at the expense of more complex units and vice versa. In a similar manner, unit adaptation could be substituted by effective switching or combination mechanism. These trade-offs have interesting theoretical implications.

It has been suggested that the MOSAIC structure can be interpreted as a time-varying RBF (Radial Base Function) network [18]. Compared to a conventional RBF network, MOSAIC uses functions of inputs instead of constant coefficients and the center points are the next desired points and therefore time variant. Although potentially much more complex functions could be estimated by a time-varying RBF network, it is not clear how we can harness its power. For example by using linear forward models, it is easy to verify the approximation capability of this network is not different than a locally weighted projection regression (LWPR) [78].

5.3 Possible Solutions

To address some of these problems, we take advantage of a few known control approaches. First of all, the neural circuitry and specifically the inverse controllers in the MOSAIC model could be replaced by adaptive filters. In fact, CBFELM proposed by Kawato is quite compatible to this view. Also, Schweighofer-Arbib model [64, 65] could similarly be analyzed in the framework proposed by Sanner and Slotine [63]. They have proposed approximation of the non-linear state transition matrix and adaptation of parameters. Moreover, from computational point of view the cerebellar circuitry could be represented by a two layer artificial neural network consisting of a layer of granule cells and a layer of Purkinje cells.

As a partitioning principle, it is possible to consider linearization technique around different operating points and switching between them. This is in fact equivalent to different subtasks. Functional modules can be realized by having ideal inverse models with different initial parameters. Additionally, the combination of these two techniques is possible.

In order to solve the problem of switching back and forth and poor combination, we can introduce prior probabilities to take into account temporal continuity or spatial locality. Also Hidden Markov Model (HMM) is able to model probability transitions in a much more efficient way. To solve the problem with the distribution of modules, ideas from self-organizing networks could be borrowed and simulated annealing of parameters could be considered. Another way to improve the performance is that to ensure that the error in a forward model prediction follows the error in the corresponding inverse model i.e. the module which has the lowest error in prediction should produce the lowest error in control.

Though the problems of choosing a controller and a combination method are not totally independent, the following list summarizes the pros and cons of some of the choices discussed above or used in the variants of MOSAIC (refer to Section 3.1).

What controller?

- Simplified Cellular structure

+ Not much different than a 2 layer ANN
+ Compatible with FEL
- Requires more work on stability

- RBF Neural Network

  + Generic non-linear (NL) function approximator
  + Compatible with FEL
  + Stability could be addressed

- Adaptive Computed Torque

  + Simple implementation
  + compatible with FEL and able to cope with delay
  - Calculation of nonlinear functions are biologically implausible

- LQR

  + Strong support from control
  + Fairly simple to calculate
  + Lend itself to linearization technique
  - No adaptation
  - Violates internal model

- Linear with adaptation

  + Compatible with FEL
  - Lack of theory for NL plant and combination strategy
  - Stability

What combining algorithm?

- Original MOSAIC

  - Based on instantaneous error so jittery
  - Sensitive to sigma parameter
  - No of modules are manually tuned
  - Inefficient distribution of resp. among modules

- HMM MOSAIC

  - heavy computation
  - Fixed to linear forward models
  - Originally in batch mode (possible to be made online)
  + improved parameter tuning and resp. estimation by EM

- eMOSAIC

  + Better resp. through prior probability (temporal continuity constraint)

- AMA-MOSAICI
  + Linear clustering algorithm to split the trajectory to subtasks

Chapter 6

Integrated Model

Figure 6.1 is the block diagram of the complete plant. It highlights the building blocks and the assumed variables.

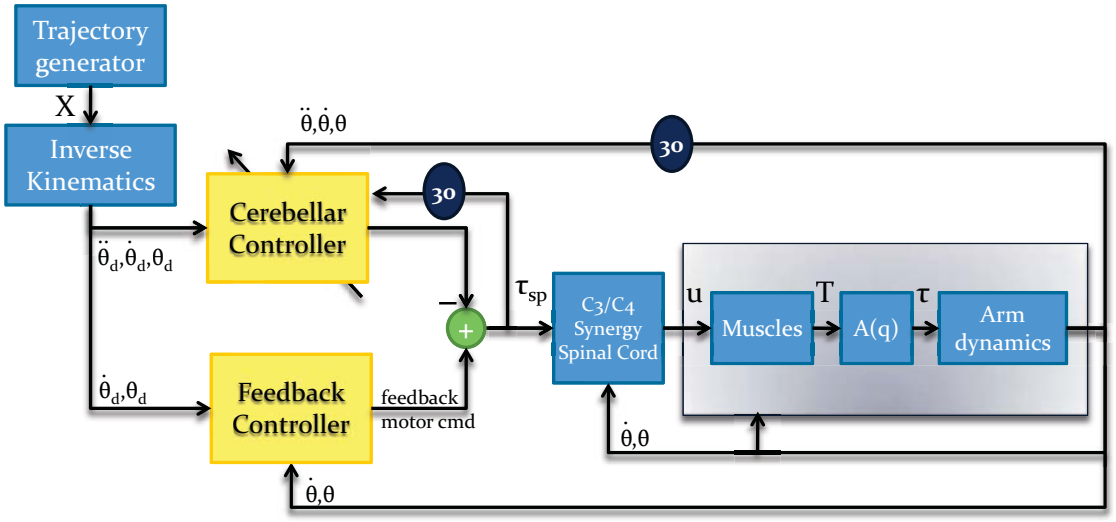

Figure 6.1: A high level structure of the complete control loop. X denotes the desired position in the task space, θ and τ_{sp} are defined in the joint space and denote the angular position and the torque sent to the minimum tension algorithm respectively. The vector of muscle activations is represented by u and T shows the tensions across the muscles.

Figure 6.2 is a customized cerebellar controller which is used for the final experiments. Since each module in this model has a signature receptive field for its training, we call it ORF-MOSAIC (Organized by Receptive Fields MOSAIC). Other variations which were used in the project appear in the appendix.

6.1 Assumptions

Here, the assumptions of our models are summarized. Similar assumptions are commonly made and they are partly supported by biological evidences.

- The motor cortex is responsible for trajectory planning in the form of minimum jerk [19]

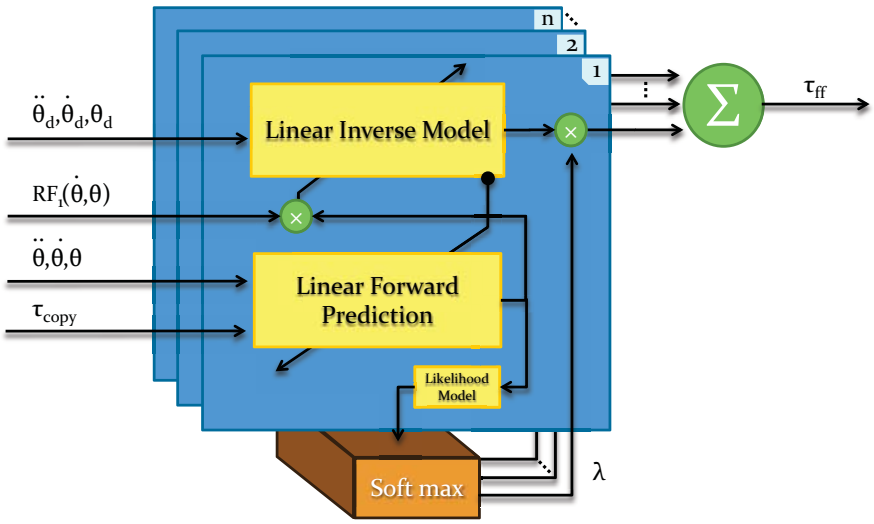

Figure 6.2: ORF-MOSAIC structure, $\mathrm{RF}_n(\dot{\theta}, \theta)$ indicates receptive field function, θ_d desired trajectory, θ feedback signals, τ_{copy} command send to the plant, λ responsibility signal, the forward prediction block is paired to the inverse model therefore uses the same parameters

- Planning is done in task space, control in joint space and there is a transformation to muscle space [64] (for joint based control see [67])
- The cerebellum builds internal models so that after learning control is done by inverse models [47]
- The sensory system through either proprioceptive or cutaneous receptors is able to provide an estimate of joint angles, angular velocity and acceleration [37, 5]
- Muscle coactivation works in a way that in an agile motion the total tension across muscles is minimized

Also for the modules, according to the discussion in the previous chapter, we chose to examine the function based and the state based modules. To arrive at the final design, we experimented with the FEL controller [25] and the adaptive controller based on Slotine's work [70, 69] as the control modules.

6.2 Implementation

Matlab and Simulink were used for implementation of the algorithms. We also benefit from some routines in Robotic Toolbox [11]. In the rest of this section, some details of the implementation are described.

6.2.1 Forward and Inverse Kinematics

In case of a simple two link model of an arm, both the forward and the inverse kinematics is possible to be computed geometrically. Specifically, the position of the hand is determined by:

$$\mathbf{p}_{EE} = \begin{bmatrix} l_1 \cos(\theta_1) + l_2 \cos(\theta_1 + \theta_2) \\ l_1 \sin(\theta_1) + l_2 \sin(\theta_1 + \theta_2) \end{bmatrix} \tag{6.1}$$

The inverse kinematics is about finding the joint space variables given the task space variables. Even for the simple case of two link manipulator, the angles are not unique i.e. for every end effector's position, there are two sets of angles. However, because of the limitation in the joints of human arm we can ignore one of the solution. Accordingly

$$\theta_2 = +\text{atan}\sqrt{\frac{(l_1 + l_2)^2 - (x^2 + y^2)}{(x^2 + y^2) - (l_1 - l_2)^2}} \tag{6.2}$$

$$\theta_1 = \text{atan2}\left(x(l_1 + l_2\cos(\theta_2)) + y l_2 \sin(\theta_2), y(l_1 + l_2\cos(\theta_2)) - x l_2 \sin(\theta_2)\right), \tag{6.3}$$

where atan2 is four quadrant arctangent function.

On the contrary, even for extra degrees of freedom, the speed of the end effector is uniquely determined by multiplication of the velocities in the task space by the inverse of the geometrical Jacobian matrix.

$$\mathbf{V} = \mathbf{J}_e \dot{\boldsymbol{\theta}} \tag{6.4}$$

$$\mathbf{J}_e = \begin{bmatrix} -l_1 \sin(\theta_1) - l_2 \sin(\theta_1 + \theta_2) & -\sin(\theta_1 + \theta_2) l_2 \\ l_1 \cos(\theta_1) + l_2 \cos(\theta_1 + \theta_2) & l_2 \cos(\theta_1 + \theta_2) \end{bmatrix} \tag{6.5}$$

Similarly, by taking derivative of Equation 6.4, we can derive the relation between the acceleration in the task space and the joint space.

$$\mathbf{a} = \frac{d\mathbf{V}}{dt} = \dot{\mathbf{J}}\dot{\boldsymbol{\theta}} + \mathbf{J}\ddot{\boldsymbol{\theta}} = \begin{bmatrix} \dot{\boldsymbol{\theta}}^T \mathbf{H}(x) \dot{\boldsymbol{\theta}} \\ \dot{\boldsymbol{\theta}}^T \mathbf{H}(y) \dot{\boldsymbol{\theta}} \end{bmatrix} + \mathbf{J}\ddot{\boldsymbol{\theta}}, \tag{6.6}$$

where $\mathbf{H}()$ is the Hessian matrix with respect to the variable indicated in parentheses.

6.2.2 Desired Trajectory

According to our assumptions, the desired trajectory in the task space follows the minimum jerk principle. The solution to minimum jerk for traveling between two points is basically a fifth order polynomial [68]. If we set the boundary conditions for the starting and end positions and velocities and accelerations to zero, the following equations are obtained. In case of non-straight paths, it is possible to define via-points.

Minimizing

$$H\left(\underline{x}(t)\right) = \frac{1}{2}\int_{t=0}^{a} \left(\dddot{x}^2 + \dddot{y}^2\right) dt, \tag{6.7}$$

results in

$$\underline{x}(t) = \begin{pmatrix} x_i + (x_f - x_i)\left(10(t/a)^3 - 15(t/a)^4 + 6(t/a)^5\right) \\ y_i + (y_f - y_i)\left(10(t/a)^3 - 15(t/a)^4 + 6(t/a)^5\right) \end{pmatrix} \tag{6.8}$$

6.2.3 Minimum Tension Control

According to our assumptions and the discussion in Section 5.1, a transformation between joint space and muscle space must exist. In an agile movement, it is assumed to follow a minimum tension principle.

$$\underset{u}{\text{minimize}}\ \frac{1}{2}T^T T \text{ subject to } 0 \leq u \leq 1 \text{ and } \tau = \tau_{sp} \tag{6.9}$$

Since the vector of tensions T is a 2nd degree function of u, the problem could be posed as convex optimization. However, due to simple structure of the equations, it is possible to solve it with quadratic programming [23] in the following generic form:

$$\underset{x}{\text{minimize}}\ \frac{1}{2}x^T H x + f^T x \text{ subject to } Ax \leq b. \tag{6.10}$$

Let's define

$$B = -A(\theta)^T \tag{6.11}$$

By orthogonal decomposition of T, we get

$$T = T_m + T_\perp \alpha \tag{6.12}$$

$$T_m = B^\dagger \tau_{sp} \tag{6.13}$$

$$T_\perp = I_{6\times 6} - B^\dagger B, \tag{6.14}$$

where $B^\dagger$ is the Moore-Penrose pseudo inverse of B and $\alpha \in \mathbb{R}^6$ is an arbitrary vector.

Substituting (6.12) into the optimization problem results in:

$$\begin{aligned}\frac{1}{2}T^T T =& \frac{1}{2}\left(T_m + T_\perp \alpha\right)^T \left(T_m + T_\perp \alpha\right) \\ =& \frac{1}{2}\alpha^T T_\perp^T T_\perp \alpha + \left(T_\perp^T T_m\right)^T \alpha.\end{aligned} \tag{6.15}$$

Since T is a convex function of u, we observe that its maximum and minimum in the range of the allowable muscle activation ($0 \leq u \leq 1$) lie either at the extremum points or the border points. Additionally, rows of T are independents, i.e., each row is only a function of one element of u. Therefore, by limiting T between theses values we can guarantee that u is within the range.

$$T > \min\left(T_0, T_1, T_x\right) \Rightarrow T_\perp \alpha < -\min\left(T_0, T_1, T_x\right) + T_m \tag{6.16}$$

$$T < \max\left(T_0, T_1, T_x\right) \Rightarrow T_\perp \alpha < \max\left(T_0, T_1, T_x\right) - T_m \tag{6.17}$$

Here, T_0, T_1, and T_x corresponds to the tension with uniformly null activations, one, and activation corresponding to the extrema of (3.18) respectively.

Consequently, the constraints could be written as follows:

$$A = \begin{pmatrix} -T_\perp \\ T_\perp \end{pmatrix},\ b = \begin{pmatrix} T_m - \min\left(T_0, T_1, T_x\right) \\ -T_m + \max\left(T_0, T_1, T_x\right) \end{pmatrix}, \tag{6.18}$$

which results in the final quadratic programming problem,

$$\underset{\alpha}{\text{minimize}}\ \frac{1}{2}\alpha^T T_\perp^T T_\perp \alpha + \left(T_\perp^T T_m\right)^T \alpha \text{ subject to } A\alpha \leq b. \tag{6.19}$$

After finding α, the optimum tension vector is calculated by (6.12), and u is uniquely determined by (3.18).

6.2.4 Adaptive Controller (Slotine)

This scheme effectively exploits some particular structure of a manipulator's dynamics. Accordingly, it results in simple stable algorithm which requires neither feedback of joint accelerations nor inversion of the estimated inertia matrix [70, 69]. In this approach, a reference trajectory is introduced to restrict the residual error to lie on a sliding surface. This guarantees that position error as well as velocity errors converge to zero (see [39] for a critique of the proofs). $\mathbf{K}_P$ and $\mathbf{\Gamma}$ are symmetric positive definite matrices, usually diagonal. In joint space the controller equations are

$$\tilde{\mathbf{q}}(t) = \mathbf{q}(t) - \mathbf{q}_d(t) \tag{6.20}$$
$$\dot{\mathbf{q}}_r = \dot{\mathbf{q}}_d - \mathbf{\Lambda}\tilde{\mathbf{q}} \tag{6.21}$$
$$\ddot{\mathbf{q}}_r = \ddot{\mathbf{q}}_d - \mathbf{\Lambda}\dot{\tilde{\mathbf{q}}} \tag{6.22}$$
$$\mathbf{s} = \dot{\tilde{\mathbf{q}}}_r = \dot{\mathbf{q}} - \dot{\mathbf{q}}_r = \dot{\tilde{\mathbf{q}}} + \mathbf{\Lambda}\tilde{\mathbf{q}} \tag{6.23}$$

The control law and adaptation law are

$$\boldsymbol{\tau} = \hat{\mathbf{H}}(\mathbf{q})\ddot{\mathbf{q}}_r + \hat{\mathbf{C}}(\mathbf{q}, \dot{\mathbf{q}})\dot{\mathbf{q}}_r + \hat{\mathbf{G}}(\mathbf{q}) - \mathbf{K}_D\mathbf{s} \tag{6.24}$$
$$\dot{\hat{\mathbf{a}}} = -\mathbf{\Lambda}^{-1}\mathbf{Y}^T(\mathbf{q}, \dot{\mathbf{q}}, \dot{\mathbf{q}}_r, \ddot{\mathbf{q}}_r)\,\mathbf{s}, \tag{6.25}$$

where $\mathbf{Y}$ is defined so that

$$\mathbf{Y}(\mathbf{q}, \dot{\mathbf{q}}, \dot{\mathbf{q}}_r, \ddot{\mathbf{q}}_r)\,\hat{\mathbf{a}} = \hat{\mathbf{H}}(\mathbf{q})\ddot{\mathbf{q}}_r + \hat{\mathbf{C}}(\mathbf{q}, \dot{\mathbf{q}})\dot{\mathbf{q}}_r + \hat{\mathbf{G}}(\mathbf{q}) \tag{6.26}$$

If we drop the boldface notation for simplicity, we find the following equations for a simple two-link manipulator:

$$H(q)\ddot{q} + C(q, \dot{q})\dot{q} = \tau \tag{6.27}$$

$$H = \begin{pmatrix} a_1 + 2a_3\cos(q_2) + a_2 & a_3\cos(q_2) + a_2 \\ a3\cos(q_2) + a_2 & a_2 \end{pmatrix} \tag{6.28}$$

$$C = \begin{pmatrix} -a_3\sin(q_2)\dot{q}_2 & -a_3\sin(q_2)(\dot{q}_1 + \dot{q}_2) \\ a_3\sin(q_2)\dot{q}_1 & 0 \end{pmatrix} \tag{6.29}$$

$$a_1 = m_2 l_1^2 + m_1 r_1^2 + I_1 \tag{6.30}$$
$$a_2 = m_2 r_2^2 + I_2 \tag{6.31}$$
$$a_3 = m_2 l_1 r_2 \tag{6.32}$$

Using the notation of $c_2 = \cos(q_2)$ and $s_2 = \sin(q_2)$,

$$Y(q, \dot{q}, \dot{q}_r, \ddot{q}_r) = \begin{bmatrix} Y_{11} & Y_{12} & Y_{13} \\ 0 & Y_{22} & Y_{23} \end{bmatrix} \tag{6.33}$$

$$Y_{11} = \ddot{q}_{r1},\ Y_{12} = \ddot{q}_{r1} + \ddot{q}_{r2} \tag{6.34}$$
$$Y_{13} = 2c_2\ddot{q}_{r1} + c_2\ddot{q}_{r2} - s_2\dot{q}_2\dot{q}_{r1} - s_2\dot{q}_{r2}\dot{q}_1 - s_2\dot{q}_2\dot{q}_{r2} \tag{6.35}$$
$$Y_{22} = \ddot{q}_{r1} + \ddot{q}_{r2},\ Y_{23} = c_2\ddot{q}_{r1} + s_2\dot{q}_{r1}\dot{q}_1 \tag{6.36}$$

6.2.5 FEL Controller

Using small-gain theorem and Lyapunov stability theorem, the authors in [76] have developed a framework for analysis of the stability of FEL with time delay in the feedback loop. The result has been derived for a two-link manipulator and a posssible extension to other non-linear systems has been suggested. In addition, it has been claimed that such structure is able to cope with delays up to 200 milliseconds in practice.

Assuming that $K_{fb} = -[K_1 K_2]$ is stabilizing for a well-tuned system (no error in estimated parameters) and for given time delay d, and additionally $H(\theta)K_2 = K_2 H(\theta)$, they have shown that the adaptive control system is globally asymptotically stable [76].

Here is the derivation of the required controller for the two link arm structure.

$$Y(q, \dot{q}, \ddot{q}) = \begin{bmatrix} Y_{11} & Y_{12} & Y_{13} \\ 0 & Y_{22} & Y_{23} \end{bmatrix} \tag{6.37}$$

$$Y_{11} = \ddot{q}_1,\ Y_{12} = \ddot{q}_1 + \ddot{q}_2 \tag{6.38}$$
$$Y_{13} = 2\ddot{q}_1 \cos(q_2) + \cos(q_2)\ddot{q}_2 - 2\dot{q}_1\dot{q}_2 \sin(q_2) - \dot{q}_2^2 \sin(q_2) \tag{6.39}$$
$$Y_{22} = \ddot{q}_1 + \ddot{q}_2,\ Y_{23} = \ddot{q}_1 \cos(q_2) + \dot{q}_1^2 \sin(q_2) \tag{6.40}$$

In order to model an external field in the form of Equation 6.41, we extend the parameters as follows.

$$f = B\dot{q}, \tag{6.41}$$

where f is force vector, $\dot{q}$ the angular velocity vector, and B is a constant matrix representing viscosity of the environment in the joint space.

$$B = \begin{bmatrix} b_1 & b_2 \\ b_3 & b_4 \end{bmatrix} \tag{6.42}$$

$$\mathbf{a} = (a_1, a_2, a_3, b_1, b_2, b_3, b_4) \tag{6.43}$$

and the required

$$Y(q, \dot{q}, \ddot{q}) = \begin{bmatrix} Y_{11} & Y_{12} & Y_{13} & Y_{14} & Y_{15} & 0 & 0 \\ 0 & Y_{22} & Y_{23} & 0 & 0 & Y_{26} & Y_{27} \end{bmatrix} \tag{6.44}$$

$$Y_{11} = \ddot{q}_1,\ Y_{12} = \ddot{q}_1 + \ddot{q}_2 \tag{6.45}$$
$$Y_{13} = 2\ddot{q}_1 \cos(q_2) + \cos(q_2)\ddot{q}_2 - 2\dot{q}_1\dot{q}_2 \sin(q_2) - \dot{q}_2^2 \sin(q_2) \tag{6.46}$$
$$Y_{14} = \dot{q}_1,\ Y_{15} = \dot{q}_2 \tag{6.47}$$
$$Y_{22} = \ddot{q}_1 + \ddot{q}_2 \tag{6.48}$$
$$Y_{23} = \ddot{q}_1 \cos(q_2) + (\dot{q}_1^2) \sin(q_2) \tag{6.49}$$
$$Y_{26} = \dot{q}_1,\ Y_{27} = \dot{q}_2 \tag{6.50}$$
$$\tag{6.51}$$

6.2.6 Improving Responsibility Signal

As discussed earlier, when we are dealing with a few modules, it is required that the prediction error indicate correctly the error in the output of the corresponding inverse model. Forward models could act as observer and predict the current system state. In continuous formulation, another possibility is to consider an estimate of the acceleration, $\hat{\dot{\mathbf{q}}}$, as the output of the forward models. No matter how forward modules partition the space, it is reasonable that their prediction quality covary with the control quality of the respective inverse models.

Consider the simplified equation of the motion.

$$\boldsymbol{\tau} = \mathbf{H}(\mathbf{q})\ddot{\mathbf{q}} + \mathbf{C}(\mathbf{q}, \dot{\mathbf{q}})\dot{\mathbf{q}} \tag{6.52}$$

In case of a FEL controller, the torque after perfect adaptation and the estimated one based on the current parameters result in the following equations.

$$\begin{aligned}
\boldsymbol{\tau}^o =& \mathbf{H}(\mathbf{q}_d)\ddot{\mathbf{q}}_d + \mathbf{C}(\mathbf{q}_d, \dot{\mathbf{q}}_d)\dot{\mathbf{q}}_d && (6.53)\\
\hat{\boldsymbol{\tau}} =& \hat{\mathbf{H}}(\mathbf{q}_d)\ddot{\mathbf{q}} + \hat{\mathbf{C}}(\mathbf{q}_d, \dot{\mathbf{q}}_d)\dot{\mathbf{q}}_d && (6.54)\\
\boldsymbol{\tau}^o - \hat{\boldsymbol{\tau}} =& \left[\mathbf{H}(\mathbf{q}_d) - \hat{\mathbf{H}}(\mathbf{q}_d)\right]\ddot{\mathbf{q}}_d + \left[\mathbf{C}(\mathbf{q}_d, \dot{\mathbf{q}}_d) - \hat{\mathbf{C}}(\mathbf{q}_d, \dot{\mathbf{q}}_d)\right]\dot{\mathbf{q}}_d && (6.55)
\end{aligned}$$

Similarly, we can calculate the error in the prediction of forward models.

$$\begin{aligned}
\ddot{\mathbf{q}} =& \mathbf{H}^{-1}(\mathbf{q})\boldsymbol{\tau} - \mathbf{H}^{-1}\mathbf{C}(\mathbf{q}, \dot{\mathbf{q}})\dot{\mathbf{q}} && (6.56)\\
\hat{\ddot{\mathbf{q}}} =& \hat{\mathbf{H}}^{-1}(\mathbf{q})\boldsymbol{\tau} - \hat{\mathbf{H}}^{-1}(\mathbf{q})\hat{\mathbf{C}}(\mathbf{q}, \dot{\mathbf{q}})\dot{\mathbf{q}} && (6.57)\\
\ddot{\mathbf{q}} - \hat{\ddot{\mathbf{q}}} =& \ddot{\mathbf{q}} - \hat{\mathbf{H}}^{-1}(\mathbf{q})\left(\mathbf{H}(\mathbf{q})\ddot{\mathbf{q}} + \mathbf{C}(\mathbf{q}, \dot{\mathbf{q}})\dot{\mathbf{q}}\right) + \hat{\mathbf{H}}^{-1}(\mathbf{q})\hat{\mathbf{C}}(\mathbf{q}, \dot{\mathbf{q}})\dot{\mathbf{q}} && (6.58)\\
=& \ddot{\mathbf{q}} - \hat{\mathbf{H}}^{-1}(\mathbf{q})\mathbf{H}(\mathbf{q})\ddot{\mathbf{q}} - \hat{\mathbf{H}}^{-1}(\mathbf{q})\left(\mathbf{C}(\mathbf{q}, \dot{\mathbf{q}}) - \hat{\mathbf{C}}(\mathbf{q}, \dot{\mathbf{q}})\right)\dot{\mathbf{q}} && (6.59)
\end{aligned}$$

By comparing Equation 6.55 and 6.59, we see that the multiplication of the prediction error by $-\hat{\mathbf{H}}(\mathbf{q})$ result in a similar dynamics to Equation 6.55. If we are following the desired trajectory, they become exactly the same.

$$-\hat{\mathbf{H}}(\mathbf{q})(\ddot{\mathbf{q}} - \hat{\ddot{\mathbf{q}}}) = \left[\mathbf{H}(\mathbf{q}) - \hat{\mathbf{H}}(\mathbf{q})\right]\ddot{\mathbf{q}} + \left[\mathbf{C}(\mathbf{q}, \dot{\mathbf{q}}) - \hat{\mathbf{C}}(\mathbf{q}, \dot{\mathbf{q}})\right]\dot{\mathbf{q}} \tag{6.60}$$

To show the validity of Equation 6.60, we present the result of a simulation. The system has not yet converged as Figure 6.3 indicates. By comparing Figure 6.5 and 6.6, it is clear that the transformed error of the forward prediction correlates better with the error in the control by the inverse model.

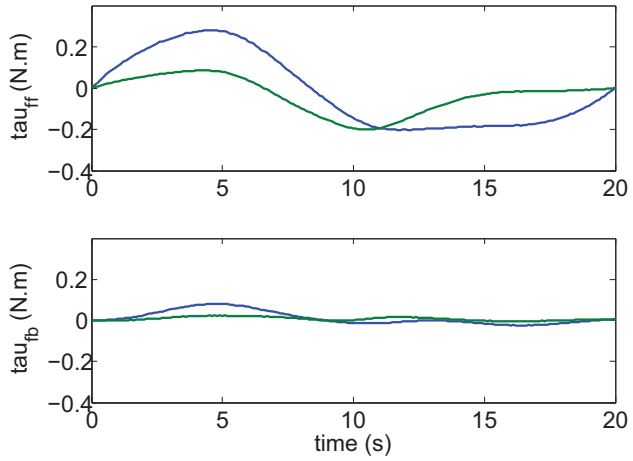

Figure 6.3: Feedforward and feedback torques before convergence to the final values

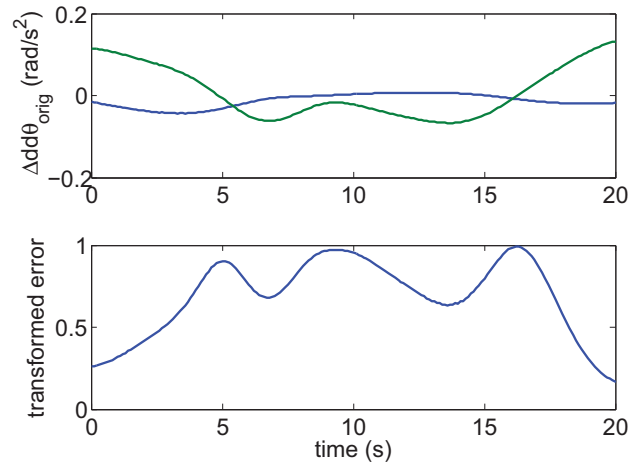

Figure 6.4: The error between the measured joint acceleration and the predicted joint acceleration

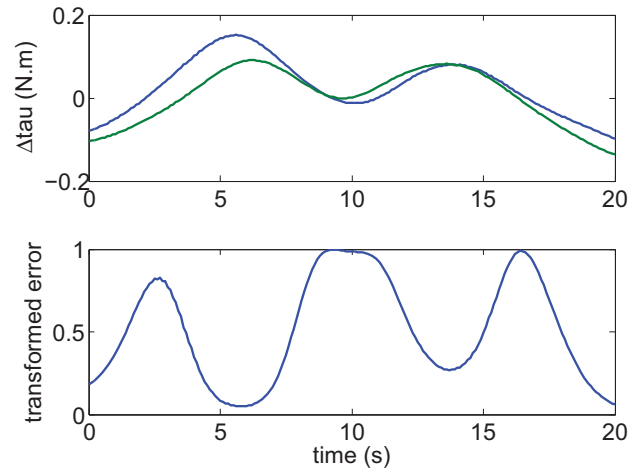

Figure 6.5: The error between the required torque and the torque produced by an inverse model paired to the forward model used in Figure 6.4

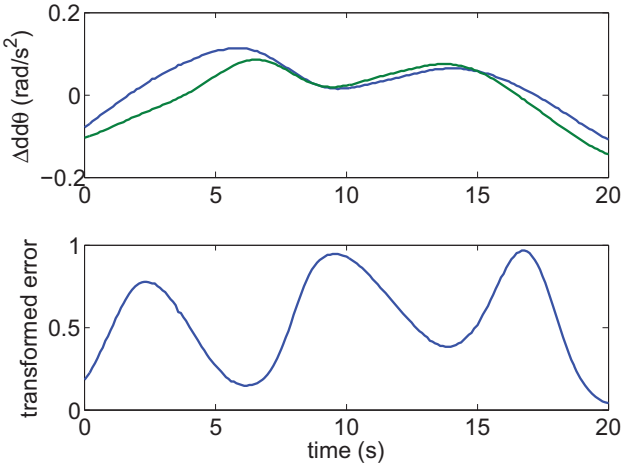

Figure 6.6: Adjusted error of forward prediction according to the Equation 6.60

6.2.7 Receptive Fields

In ORF-MOSAIC, each module has a signature receptive field modulating its training and giving rise to the organizational structure of the modules. We chose a radial base function for this purpose as below:

$$RF_i\left(x(t)\right) = e^{-(x(t)-x_i)^T \Sigma_i (x(t)-x_i)}, \tag{6.61}$$

where $x(t)$ is a vector of the states containing both θ and $\dot{\theta}$. The highest reception occures at $x(t) = x_i$ and Σ_i determines the shape of the receptive field.

Chapter 7

Experiments - Part 2

Our main aspiration in this project was to control the arm with agility and flexibility. To put it more concretely, we wished to:

- control the arm in the whole operating range
- show robustness against delay and noise in the system
- manage different loads quickly
- cope with external structured disturbance

With these targets in mind, we designed several scenarios and experiments. The assumption about coordinate transformations made it possible to divide the problem into two fairly independent subproblems. Therefore, as the first stage, we realized the transformation between the joint space to the muscle space by the minimum tension control which makes the rest of the problem similar to classical control problems.

7.1 Experimental Design

In order to test the arm individually, the torque from the computed torque method for a certain trajectory was fed into the minimum tension control algorithm in an open loop manner. We checked the validity of the solution by looking at the range of the activation signals and the resulting torque. Certainly, given the constraints in the activation signals, it is not possible to produce arbitrary torques in all states. In that case the algorithm produces a result that minimizes the worst case constraint violation and then trims it to lie in the range.

Several trajectories were experimented in the range of reasonable speed for a human. Specifically, Figure 7.1 shows extending the arm from $(90°, 120°)$ to $(30°, 30°)$ in one second.

The reset of the experiments focuses on MOSAIC model and its modules. It was important to investigate about different ways to partition the state space. Specially, functional modules and state based modules were in focus. Another dimension worth of investigation was the adaptive mechanism in relation to forward and inverse models.

It is possible to limit the adaptation to the forward model or the inverse model while the other one is paired or not. It could also be limited to certain domains such as functions or states while the rest of parameters are predetermined. Obviously, not all of the scenarios are viable. For instance, a scenario where adaptive forward models learn to partition the state space but the inverse models are fixed and there is no coupling between these two, makes no sense.

Among many possibilities, here we present the following scenarios:

1. Ideal forward models without coupling in parameters with adaptive inverse models
2. Linearized forward models without coupling in parameters with adaptive inverse models
3. Fixed linearized forward models and adaptive inverse models

The first scenario in terms of partitioning is equivalent to function based. In scenario two, both function and state based partitioning are combined. The third scenario is similar to the previous one except functions does not change and in that case new modules are required.

Moreover, different base controllers could possibly result in different responses. We experimented with linear controller and variants of FEL controller and adaptive controller of Slotine.

In the first scenario, similar behavior as discussed in Section 5.2 were observed. With random initial states, adaptation takes longer time than a single adaptive controller because of switching back and forth. However, quicker adaptation when the parameters are in the vicinity of the ideal solution was noticed. Although the system is able to quickly control a new object with parameters lying in the space spanned by the parameters of the already learned objects, one of the module eventually specializes for the new object. By variying initial states, it is also possible that one module takes over all or all modules converge to the same parameters.

The experiment with using linear models for both forward and inverse models proved inefficient. The main problem was the adaptation of 12 different parameters (for $\ddot{\mathbf{q}}_d, \dot{\mathbf{q}}_d, \mathbf{q}_d, \dot{\mathbf{q}}, \mathbf{q}, 2 \times$ offsets). It was not possible to tune these parameters in an adaptive manner. A possible solution could be training them for the whole trajectory similar to [38] which is not adaptive and consequently not the point of this work.

Finally, together with each linear forward model, a linearized version of the controller around the same operating point which only requires as many parameters as unknown parameters was used. This approach was quite effective and did not fall into the pitfall of the "curse of dimensionality."

We introduced temporal continuity as prior which overall contributed in reducing chattering effect. Also, the improvement in responsibility according to Subsection 6.2.6 seemed quite necessary.

Thanks to the linearity of the dynamics of a multi-joint body to its unknown parameters, it is possible to build incremental models. I.e. compensating only for the deviation from the ideal system.

Another idea that we considered was to make a module learn in the vicinity of a certain state irrespective of the arm's parameters. From the biological

perspective, it means that control modules are active in certain states corresponding to certain cutaneous input. From the control perspective, it means each inverse model get a chance for adaptation even if they are not controlling. This requires dissociation of control and adaptation. In this scenario since the module which learns does not contribute to the control it is not possible to use feedback signal for parameter update. Instead, we considered an estimated error in the torque which could be provided by the same technique as described in Subsection 6.2.6.

It is evident that none of the original controllers is able to counteract external fields completely since they are not equipped with the required internal model. We first established a baseline for the performance degradation. Afterwards, the parameters were extended in order to allow the controller to model constant external field in the joint space.

In order to test the complete plant, a similar setup to [67] was considered. The task was following a star pattern in a workspace centered at $(15°, 85°)$ degrees. Each movement was supposed to be carried out along a path of 10 cm and last for 0.65 sec. However, it was further allowed to settle in 0.65 sec resulting in the total experiment time of 1.3 sec. The delay from the sensory measurements was set to 30 ms. Two modules for each direction resulting in 16 modules were considered.

For the feedback controller representing joint stiffness and viscosity, the parameters were chosen in the actual measurement range specified by [54]. For Slotine's adaptive scheme:

$$\Lambda = \begin{pmatrix} 6.5 & 0.064 \\ 0.064 & 6.67 \end{pmatrix}, \; K_D = \begin{pmatrix} 2.3 & 0.9 \\ 0.9 & 2.3 \end{pmatrix} \tag{7.1}$$

and equivalently for FEL type:

$$K_P = \begin{pmatrix} 15.00 & 6.15 \\ 6.00 & 15.40 \end{pmatrix}, \; K_D = \begin{pmatrix} 2.3 & 0.9 \\ 0.9 & 2.3 \end{pmatrix} \tag{7.2}$$

In addition, the parameter of of the feedback controller representing motor cortex in the scheme of CBFELM were chosen as $K_P = 1$, $K_D = 0.5$.

A translation invariant field in the workspace for the external field was considered:

$$f = B\dot{x}, \tag{7.3}$$

where f is force vector, $\dot{x}$ the hand velocity vector, and B is a constant matrix representing viscosity of the environment in end-point coordinates. We chose B to be

$$B = \begin{bmatrix} -2.525 & -2.8 \\ -2.8 & 2.775 \end{bmatrix} \text{ N.sec/m} \tag{7.4}$$

For the test case with a load, a rod shape object orthogonally attached to the 2nd link with $m = 2$ Kg and $l = 0.6$ m was considered.

7.2 Results

Figure 7.1 shows the result of the open loop control of the arm under minimum tension condition. The algorithm has produced perfect activation signals.

The rest of the figures in this section show the performance of the cerebellar controller for different scenarios:

- A null field
  - No cerebellar controller
  - After practicing
  - Generalization to different trajectories
- With the external force field
  - No adaptation
  - After practicing
  - After effects
- Handling a new object
  - No cerebellar controller
  - Adaptation
  - After practicing

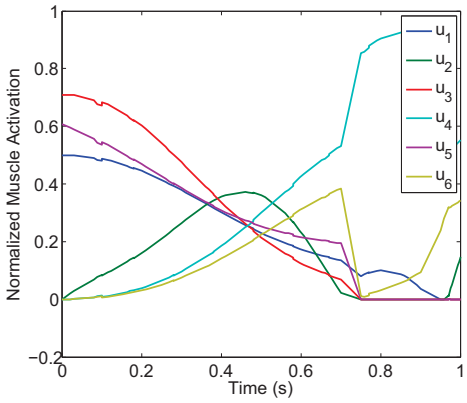

(a) Muscle activations

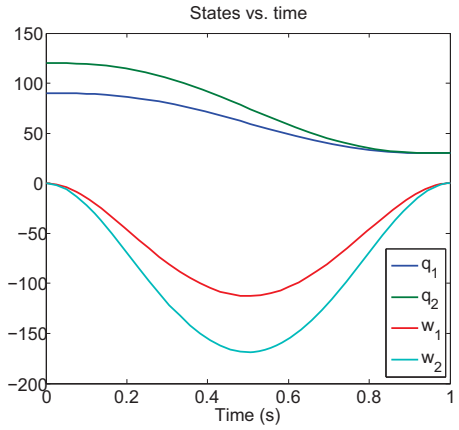

(b) Joint angles (deg) and joint angular velocities (deg/s)

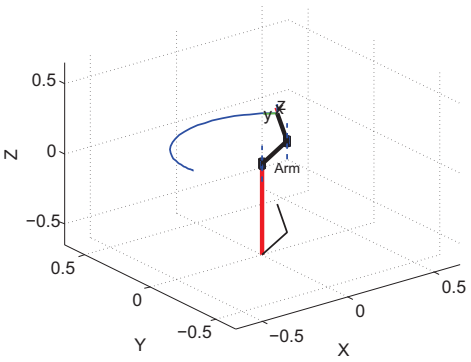

(c) Hand trajectory and final arm position

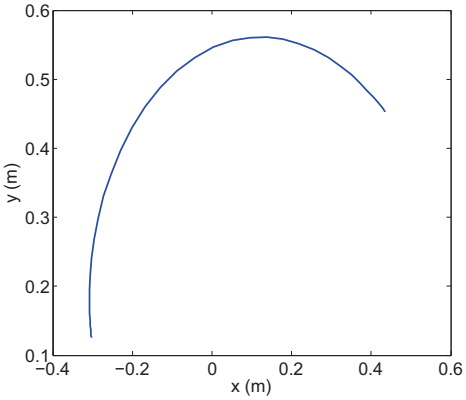

(d) Hand trajectory

Figure 7.1: Open loop control of arm with minimum tension, from $(90°, 120°)$ to $(30°, 30°)$, duration 1 sec.

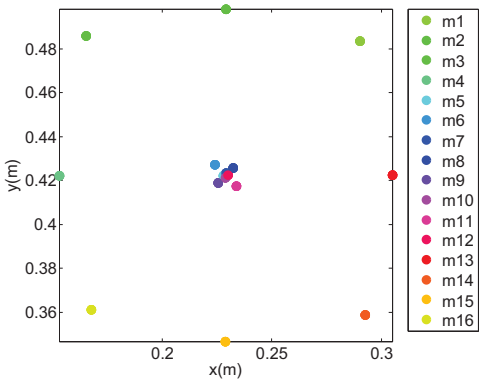

(a) Numbering and color coding of modules

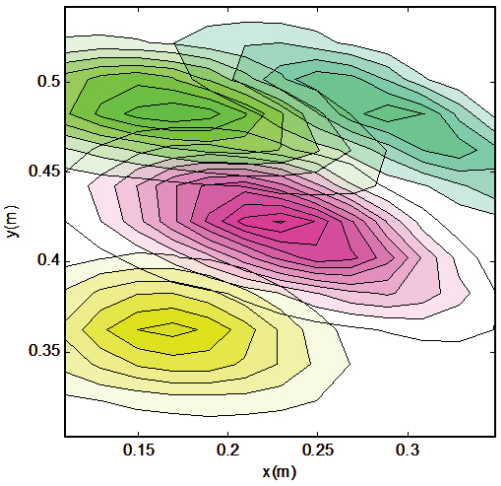

(b) Samples of receptive fields

Figure 7.2: Mapping of modules to the workspace in a static configuration

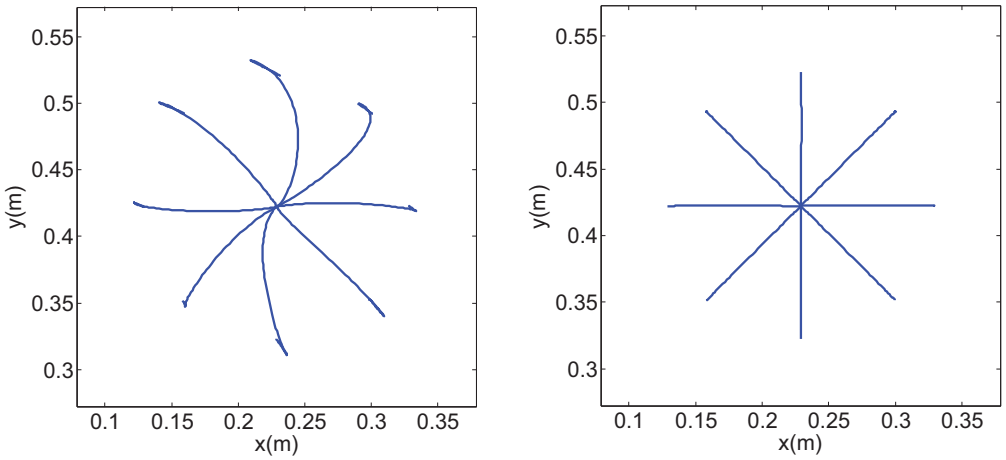

(a) (b)

Figure 7.3: (a) Hand trajectory without cerebellar control in a null force field (b)Hand trajectory after adaptation of cerebellar controller in a null field

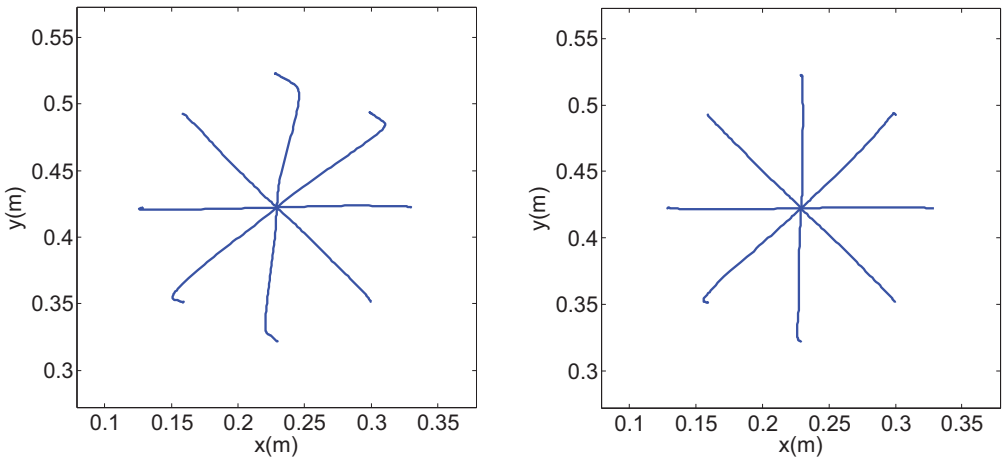

(a) (b)

Figure 7.4: (a) Disrupted hand trajectory after exposing to the force field (b)Improved hand trajectory after practicing in the force field

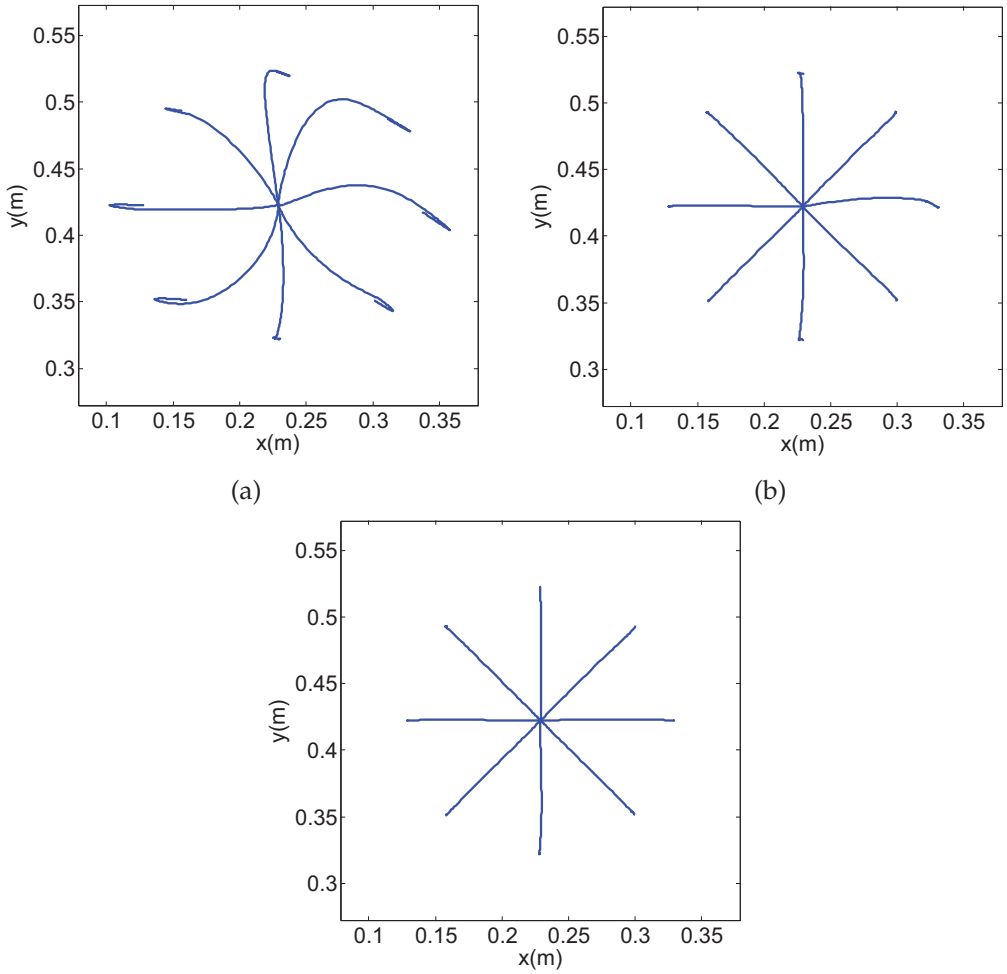

Figure 7.5: (a) Hand trajectory while carrying an object, no adaptation of the cerebellar controller (b) with adaptation of the cerebellar controller, starting from 0° and continuing clockwise (c) after practicing

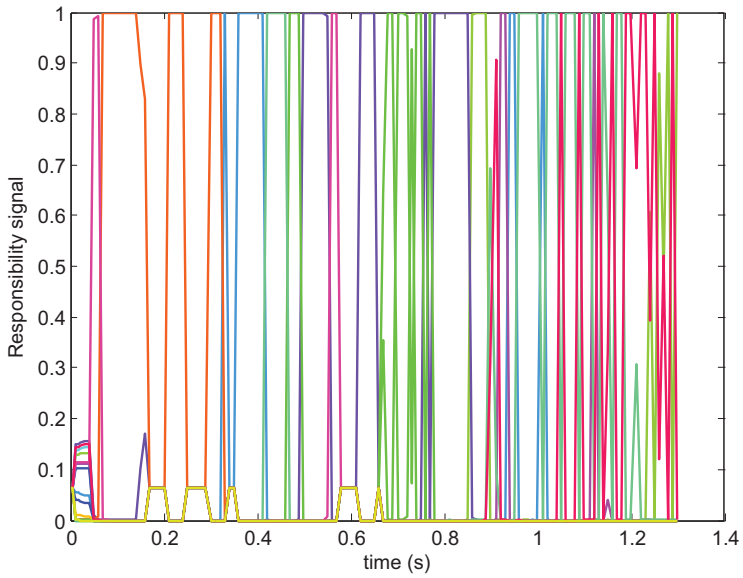

(a)

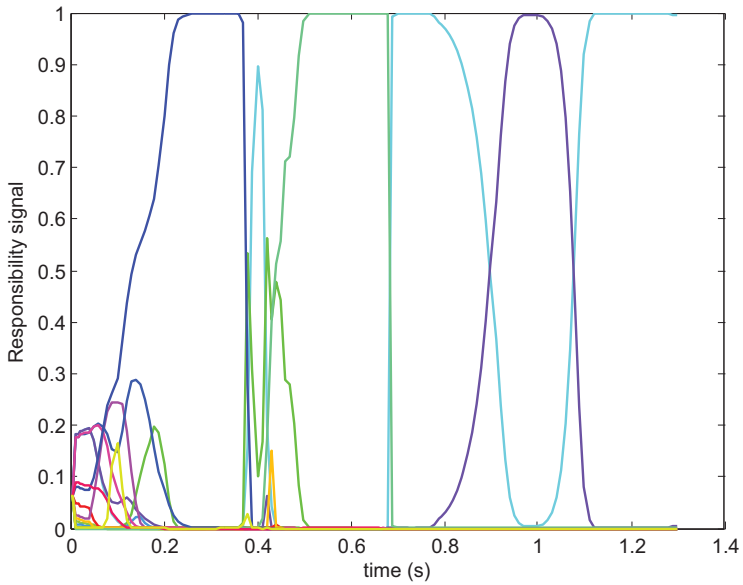

(b)

Figure 7.6: Responsibility signals for a reaching movement in 45° direction (a) before training, (b) after training.

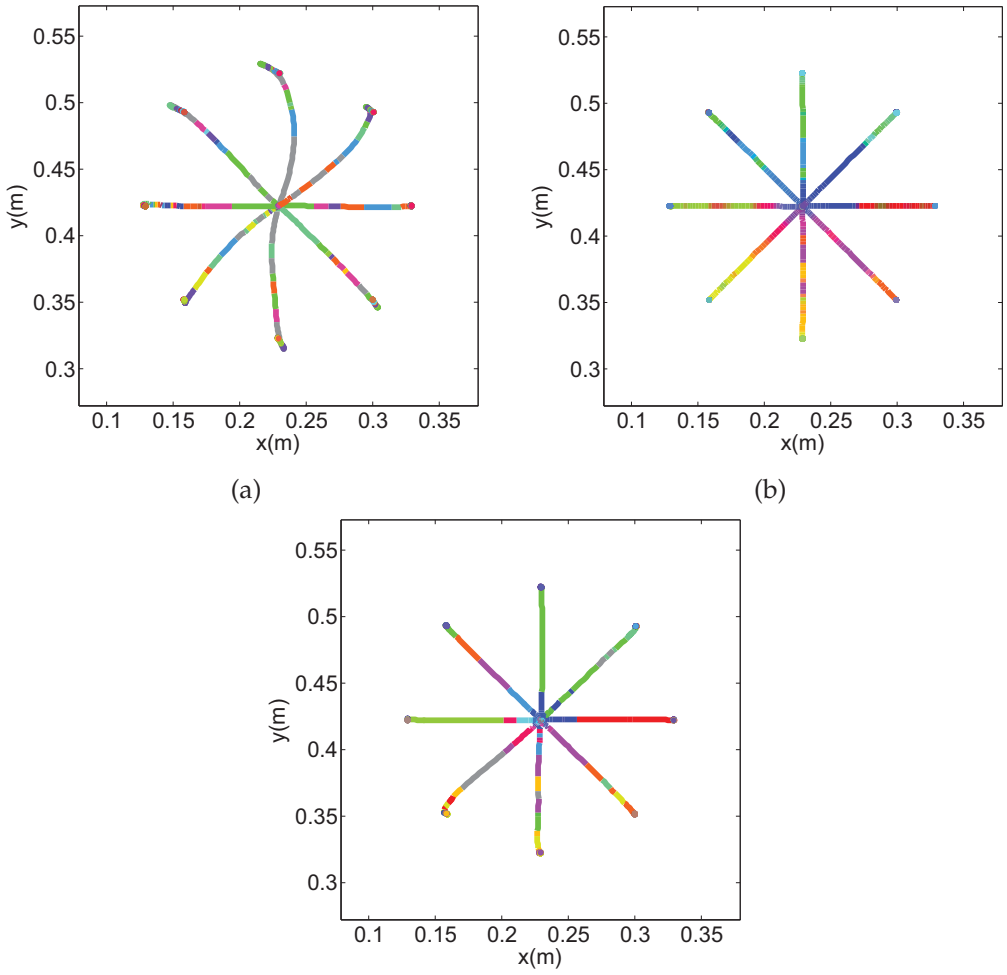

Figure 7.7: Contributing modules along the trajectory. The modules are coded with distinct colors. When they are active together the colors are combined (a) no adaptation of the cerebellar controller in a null field (b) after practicing in a null field (c) after practicing in the force field.

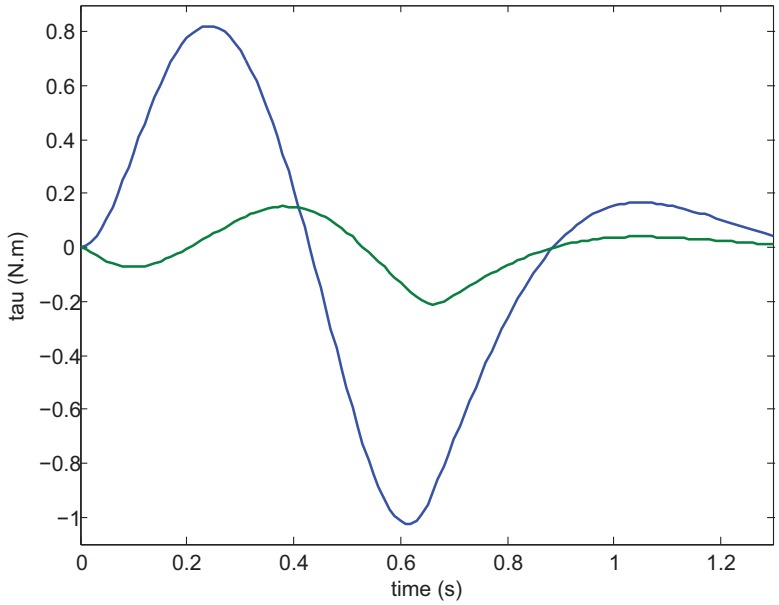

Figure 7.8: Feedback signal without the cerebellar controller, in 90° direction. The blue color corresponds to the first joint and the green color to the second joint.

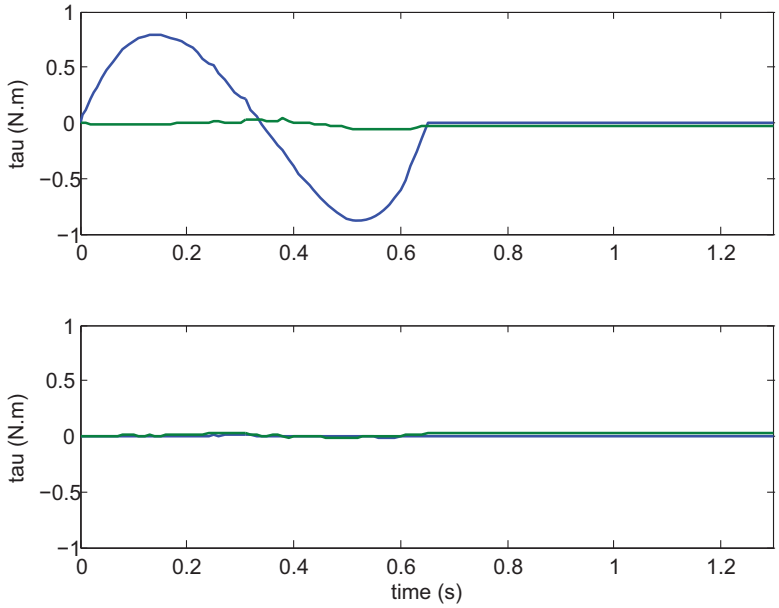

Figure 7.9: Contribution of the cerebellar controller by the feedforward, in 90° direction.

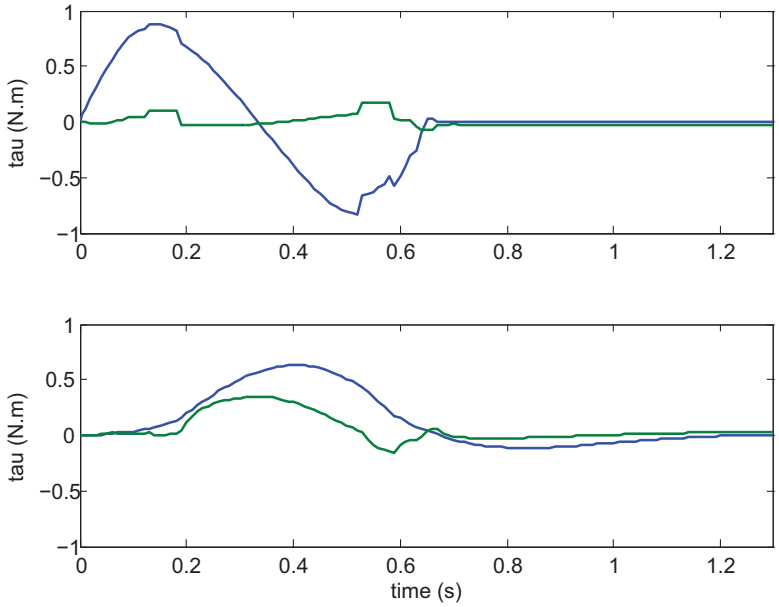

Figure 7.10: Feedforward and feedback signals upon exposure to the force field, in $90\,^{\circ}$ direction.

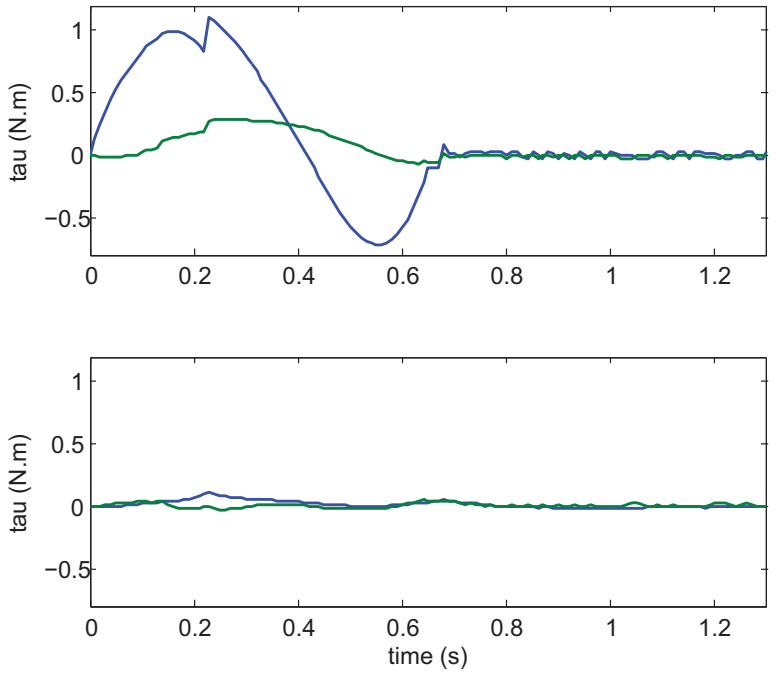

Figure 7.11: Feedforward and feedback signals after practicing in the force field, in $90\,^{\circ}$ direction.

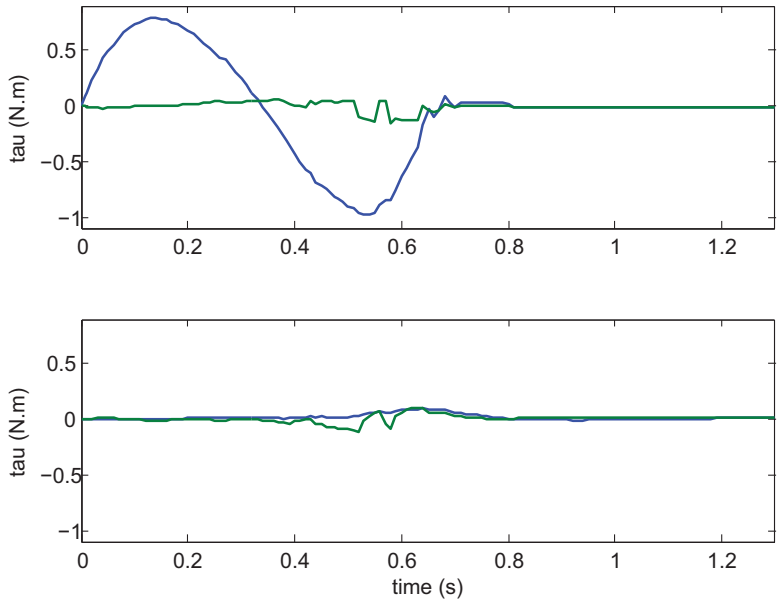

Figure 7.12: Feedforward and feedback signals after removing the force field (after effect), in 90° direction.

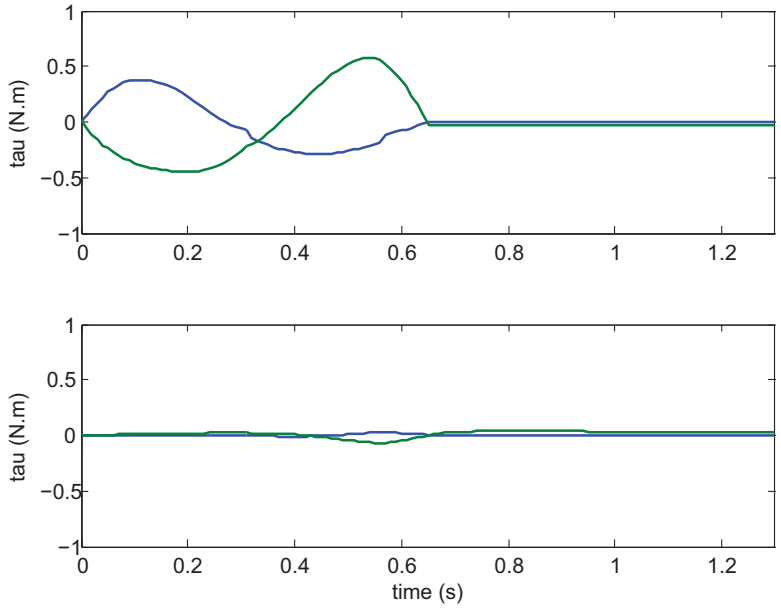

Figure 7.13: Feedforward and feedback signals after practicing while carrying the object, in 90° direction.

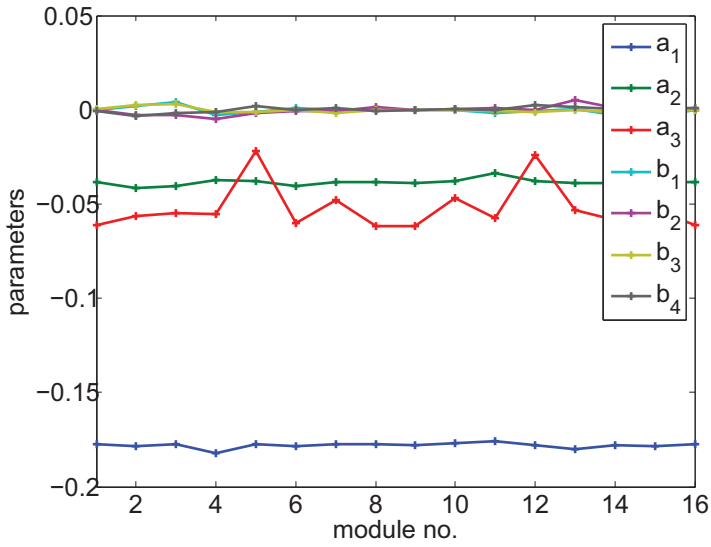

(a) Parameters in a null field

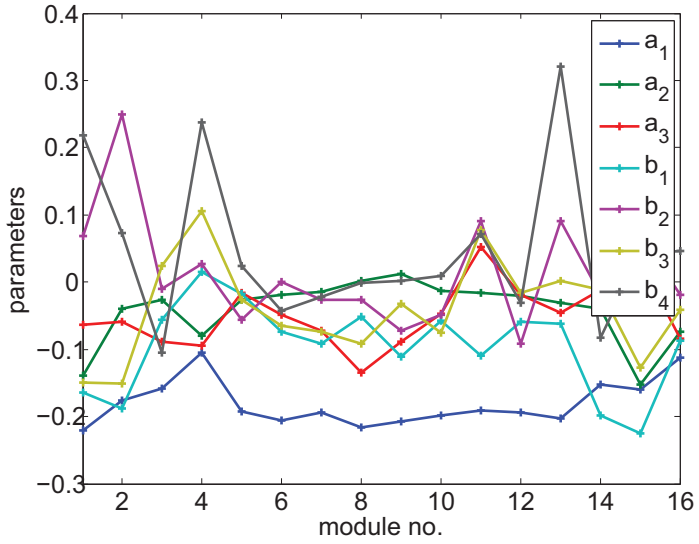

(b) Parameters in the force field

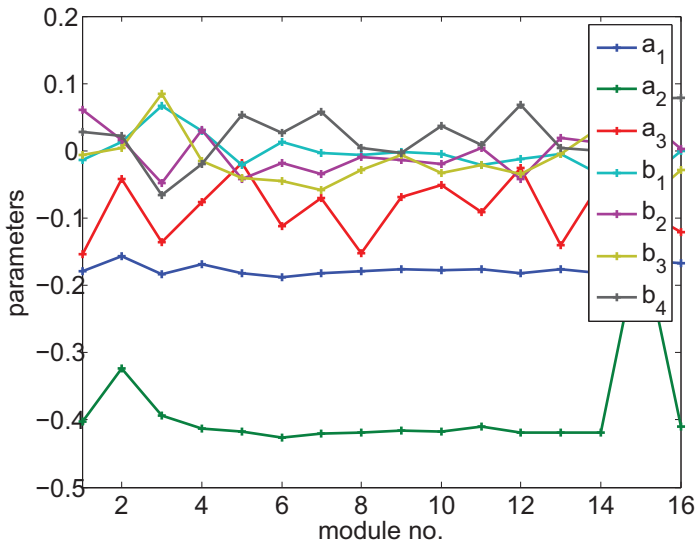

(c) Parameters while carrying the object

Figure 7.14: Parameters across modules after training

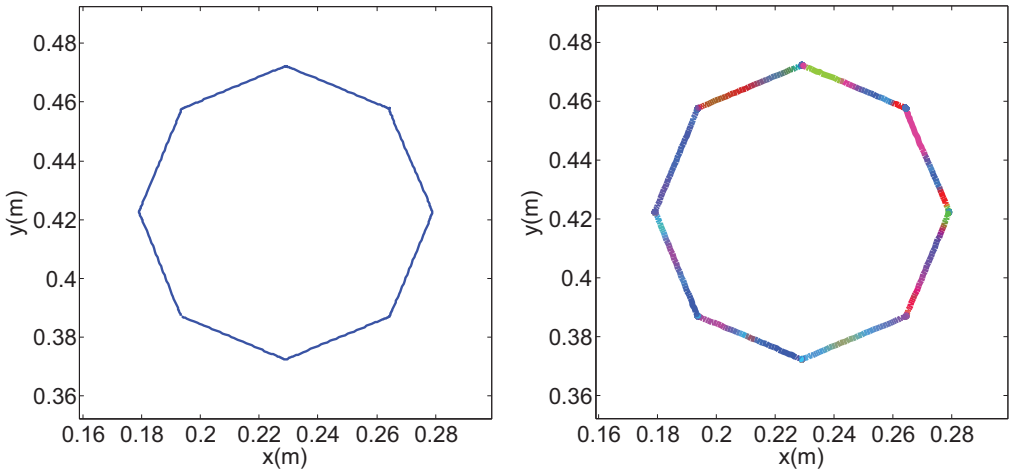

Figure 7.15: (a) Hexagon after training, (b) contribution of different modules along the path.

From Figures 7.9, 7.11, and 7.13, it is clear that the cerebellar controller has correctly learned the nonlinearities of the arm and compensated for them by the feedforward signal. Also Figures 7.7 and 7.6 show that after adaptation, the modules are activated in an orderly fashion without rapid switching. According to Figure 7.14, the parameters do not vary much across modules in a null field and reflect the physical parameters of the system. Whereas, the parameters related to the external field has distributed almost symmetrically with respect to the origin of the workspace. Figure 7.15 shows the modules are combined effectively for a different trajectory.

Chapter 8

Discussion

We did not try to optimize the receptive filed of the modules and they were selected somehow randomly at the beginning and the end of each movement. However, as the results show the system was able to correctly combine different modules in the workspace and generalize to new trajectories. Additionally, the shape of these receptive fields could be tuned by the parameters, while we considered the same weight for all joint angles and joint velocities. One way to improve this is to update these parameters in a self-organized manner. A similar method to the one proposed in [14] might be implemented.

Our formulation of the controller with 7 parameters is sufficient to compensate for a constant force field in the joint space. As we know, a constant force field in the work space varies with the joint configurations and therefore could not be compensated with the original FEL controller. However, as it was expected, partitioning the subspace with different modules allowed each of the modules to specialize in a region thus reducing the effect of the external field.

The stability of the system in the Lyapunov sense has not been investigated. It might be possible to combine the ideas from [39] with the approximate formulation of linear inverse controllers to achieve this end. Although the goal of a control system could be summarized as trajectory following, the body might take into account an optimal strategy with respect to energy consumption or other criteria. Since tensing a muscle results in an increase in its metabolism, the minimization of the tensions across muscles follows the same principle. However, optimization with a more generic perspective would require considering the task as well. To address this, simultaneous treatment of adaptation and optimal control would be the right approach [40, 41].

It is interesting to compare our results with [62]. They achieved a similar performance with 182 nodes (for two workspaces) and with as many as 1000 reaching motions while in our model only 16 modules were used and overall 16 reaching motions were enough. Furthermore, they have assumed a perfect compensation for the dynamics of the arm. Though it is evident that parameters and the complexity of the approximating functions (fully black box or gray box techniques) can affect the convergence speed, our model seems quite enough for the given tasks. It is important to note that in ORF-MOSAIC neither the parameters of the dynamic equation nor the full structure of the functions are known to the controller. Nonetheless, the system manages to adapt in a few trials and overcome the "curse of dimensionality." We believe ORF-MOSAIC

achieves this by efficiently combining different modules.

Since we do not make any predictions forward in time to compute the responsibility signals in our implementation, longer delays may affect the performance. Ideal functional modules would preserve the same performance as FEL controller, however the state-based modules gets more affected since they require an estimate of the current state.

It is possible to draw a parallel between the state based modules proposed in this work and the microzones in the cerebellum. Each module is adjusted in a certain arm configuration corresponding to certain cutaneous and proprioceptive inputs. The adjustment of parameters aims to make correction in the movement with respect to the desired trajectory. Hence, an error in the receptive field of an adjustment signal (corresponding to a climbing fiber), affect the activation of a set of muscles which would cancel it. This interpretation is in agreement with the findings about the receptive fields in the cerebellar circuitry [3, **?**]. Although, there is no clear receptive field in the input side of our model (corresponding to the parallel fibers), it is mathematically equivalent to think of the responsibility signals as the signature of such receptive fields.

Besides, forward models do not need to be a part of cerebellar controller and as it was suggested in other models [64] it could be attributed to the motor cortex. Also, we have not exactly localized the feedback controller. Instead, we have used a lump model with "safe values" corresponding to the joint stiffness and viscosity. In reality, the feedback controller might involve several loops including lower motor control with negligible delay as well as a control loop involving visual feedback with much longer delay.

Humankind uses a very conservative control strategy when encountering a new object. With regard to the functional modules, it seems reasonable to disallow switching back and forth during an initial period and use a "safe" controller instead.

Although through a couple of modifications, it was made possible to use MOSAIC model to control an arm, the author believes that it is difficult to guarantee stability in the original structure. This is mainly due to destructive effects of simultaneous adaptation in forward and inverse models. Moreover, in engineering applications it is desirable to be able to retain learned plans and therefore retrograde interference might be deleterious. Therefore, schemes such as [52] which guarantee this are preferable.

Future Works In this work, we assumed perfect transformation from joint space to muscle space according to a minimum tension principle. Evidently in a voluntary action, the CNS is able to independently control the stiffness of the arm by coactivation of muscles. This provides the CNS with another dimension of control in an advantageous way [35]. By increasing the stiffness of the arm, it is possible to improve the disturbance rejection for instance when handling an unknown object or dealing with unknown external forces. This strategy combined with adaptation can improve the overall control or even learning.

Understanding the partitioning principle of microzones in terms of kinematic and dynamic variables could add a new perspective into understanding of the cerebellar control. Simulation of skin and proprioceptive receptors could be a key to this area.

Toward satisfying more engineering objectives, it is possible to consider scenarios which combines fixed and adaptive models with reset function such as the one proposed by [57].

We found the representation of linear functions weighted by Gaussian functions as an approximation to a state transition matrix quite effective. It seems to preserve both adaptation and stability properties of the FEL algorithm [76]. If it is combined with observer type forward models (Kalman Filters), they can act as local approximation to the computed torque method. This provides an alternative formulation to [63, 62] which deserves further studies.

Chapter 9

Conclusion

A simplified model of a human arm including muscle systems was implemented. We were able to control the arm while keeping the muscle tension minimized. This allowed agile movements with minimal tension similar to a human arm. With regard to the **ORF-MOSAIC** as a cerebellar controller, it was possible to adapt to the parameters of the arm, the external field and the changes in the load carried by the arm despite moderate delay in the feedback signals received by this controller.

The new formulation offers interesting properties such as meaningful parameters compared to artificial neural networks. It has also an interesting implication for distributed control since each module only requires to know about the total contribution and not individual contributions hence makes little demand on sharing information among modules.

Though we have come far in understanding of the cerebellum and its function, it may not yet be possible to emulate it for a robotic application. Specifically, the result from the study of the MOSAIC model for the cerebellum could be summarized as below:

MOSAIC as A Control Scheme is a quite flexible structure. It might be interpreted as a generalization of some of the classical techniques. However, there is no theoretical guide for using this structure. Therefore, it must be used cautiously in conjunction with adaptation and delays.

MOSAIC as A Biological Model of the cerebellum is highly disputable. It is rather a cognitive model which might be used to describe some behavioral observations.

Bibliography

[1] Cerebellum - psychology wiki. http://psychology.wikia.com/wiki/Cerebellum, May 2011.

[2] J. S. Albus. A New Approach to Manipulator Control: the Cerebellar Model Articulation Controller (CMAC). *Journal of Dynamic Systems, Measurement, and Control*, 97:220–227, 1975.

[3] R. Apps and M. Garwicz. Anatomical and physiological foundations of cerebellar information processing. *Nature Reviews Neuroscience*, 6(4):297 – 311, 2005.

[4] M. A. Arbib, G. Metta, and P. van der Smagt. Neurorobotics: From vision to action. In B. Siciliano and O. Khatib, editors, *Springer Handbook of Robotics*, pages 1453–1480. Springer Berlin Heidelberg, 2008.

[5] E. B. Benoni. Cutaneous afferents provide information about knee joint movements in humans. *Journal of Physiology*, 531(Pt 1):289–297, 2001.

[6] E. B. Benoni and J. Niclas. Skin strain patterns provide kinaesthetic information to the human central nervous system. *Journal of Physiology*, 487(1):243–251, 1995.

[7] D. Bullock and S. Grossberg. Chapter 11 Vite and Flete: Neural Modules for Trajectory Formation and Postural Control. In W. A. Hershberger, editor, *Volitional Action - Conation and Control*, volume 62 of *Advances in Psychology*, pages 253 – 297. North-Holland, 1989.

[8] F. Campos and J. Calado. Approaches to human arm movement control–a review. *Annual Reviews in Control*, 33(1):69 – 77, 2009.

[9] C.-P. Chou and B. Hannaford. Study of human forearm posture maintenance with a physiologically based robotic arm and spinal level neural controller. *Biological Cybernetics*, 76:285–298, 1997.

[10] J. L. Contreras-Vidal, S. Grossberg, and D. Bullock. A neural model of cerebellar learning for arm movement control: cortico-spino-cerebellar dynamics. *Learning & Memory*, 3(6):475–502, Mar. 1997.

[11] P. Corke. A robotics toolbox for MATLAB. 3(1):24–32, Mar. 1996.

[12] A. d'Avella, P. Saltiel, and E. Bizzi. Combinations of muscle synergies in the construction of a natural motor behavior. *Nature Neuroscience*, 6(3):300, 2003.

[13] P. Dean, J. Porrill, C.-F. Ekerot, and H. Jörntell. The cerebellar microcircuit as an adaptive filter: experimental and computational evidence. *Nat Rev Neurosci*, 11(1):30–43, Jan 2010.

[14] P. Dean, J. Porrill, and J. V. Stone. Decorrelation control by the cerebellum achieves oculomotor plant compensation in simulated vestibulo-ocular reflex. *Proceedings of the Royal Society of London. Series B: Biological Sciences*, 269(1503):1895–1904, 2002.

[15] K. Doya, K. Samejima, K.-i. Katagiri, and M. Kawato. Multiple model-based reinforcement learning. *Neural Computation*, 14(6):1347 – 1369, 2002.

[16] T. J. Ebner. A role for the cerebellum in the control of limb movement velocity. *Current Opinion in Neurobiology*, 8(6):762 – 769, 1998.

[17] C.-F. Ekerot and H. Jörntell. Parallel fiber receptive fields: a key to understanding cerebellar operation and learning. *The Cerebellum*, 2:101–109, 2003.

[18] M. Emadi Andani, F. Bahrami, and P. Jabehdar Maralani. AMA-MOSAICI: An automatic module assigning hierarchical structure to control human motion based on movement decomposition. *Neurocomput.*, 72:2310–2318, June 2009.

[19] T. Flash. The control of hand equilibrium trajectories in multi-joint arm movements. *Biological Cybernetics*, 57:257–274, 1987.

[20] M. Fujita. Adaptive filter model of the cerebellum. *Biological Cybernetics*, 45:195–206, 1982.

[21] M. Garwicz, C.-F. Ekerot, and H. Jörntell. Organizational principles of cerebellar neuronal circuitry. *News Physiol Sci*, 13:26–32, Feb 1998.

[22] M. Garwicz, H. Jörntell, and C. F. Ekerot. Cutaneous receptive fields and topography of mossy fibres and climbing fibres projecting to cat cerebellar C3 zone. *J Physiol*, 512 (Pt 1):277–293, Oct 1998.

[23] P. E. Gill, W. Murray, and M. H. Wright. *Practical Optimization*. Academic Press, June 1981.

[24] T. Glad and L. Ljung. *Control Theory : Multivariable & Nonlinear Methods*. CRC, Mar. 2000.

[25] H. Gomi and M. Kawato. Learning control for a closed loop system using feedback-error-learning. In *Decision and Control, 1990., Proceedings of the 29th IEEE Conference on*, pages 3289 –3294 vol.6, dec 1990.

[26] H. Gomi and M. Kawato. Recognition of manipulated objects by motor learning with modular architecture networks. *Neural Networks*, 6(4):485 – 497, 1993.

[27] H. Gomi and M. Kawato. Equilibrium-point control hypothesis examined by measured arm stiffness during multijoint movement. *Science*, 272(5258):117–120, 1996.

[28] H. Gray and C. Clemente. *Anatomy of the Human Body*. Lea & Febiger, 30 edition, 1985.

[29] C. M. Harris and D. M. Wolpert. Signal-dependent noise determines motor planning. 1998.

[30] M. Haruno, D. M. Wolpert, and M. Kawato. Multiple paired forward-inverse models for human motor learning and control. In *Proceedings of the 1998 conference on Advances in neural information processing systems II*, pages 31–37, Cambridge, MA, USA, 1999. MIT Press.

[31] M. Haruno, D. M. Wolpert, and M. Kawato. Hierarchical MOSAIC for movement generation. In T. Ono, G. Matsumoto, R. Llinas, A. Berthoz, R. Norgren, H. Nishijo, and R. Tamura, editors, *Excepta Medica International Coungress Series*, volume 1250, pages 575–590, Amsterdam, The Netherlands, 2003. Elsevier Science B.V.

[32] M. Haruno, D. M. Wolpert, and M. M. Kawato. MOSAIC Model for Sensorimotor Learning and Control. *Neural Comput.*, 13:2201–2220, October 2001.

[33] H. Hatze. A mathematical model for the computational determination of parameter values of anthropomorphic segments. *Journal of Biomechanics*, 13(10):833 – 843, 1980.

[34] A. V. Hill. The Heat of Shortening and the Dynamic Constants of Muscle. *Royal Society of London Proceedings Series B*, 126:136–195, Oct. 1938.

[35] N. Hogan. Adaptive control of mechanical impedance by coactivation of antagonist muscles. 29(8):681–690, 1984.

[36] J. C. Houk, J. T. Buckingham, and A. G. Barto. Models of the cerebellum and motor learning. *Behavioral and Brain Sciences*, 19:368–383, 1996.

[37] M. Hulliger. The mammalian muscle spindle and its central control. In K. Kramer, O. Krayer, E. Lehnartz, A. v. Muralt, and H. H. Weber, editors, *Reviews of Physiology, Biochemistry and Pharmacology, Volume 101*, volume 101 of *Ergebnisse der Physiologie Biologischen Chemie und Experimentellen Pharmakologie*, pages 1–110. Springer Berlin Heidelberg, 1984.

[38] S. Jo. Letters: Adaptive biomimetic control of robot arm motions. *Neurocomput.*, 71:3625–3630, October 2008.

[39] R. Johansson. Adaptive control of robot manipulator motion. 6(4):483–490, 1990.

[40] R. Johansson. Quadratic optimization of motion coordination and control. 35(11):1197–1208, 1990.

[41] R. Johansson, P.-A. Fransson, and M. Magnusson. Optimal coordination and control of posture and movements. *J Physiol Paris*, 103(3-5):159–177, 2009.

[42] M. I. Jordan. Hierarchical mixtures of experts and the em algorithm. *Neural Computation*, 6:181–214, 1994.

[43] M. I. Jordan and D. E. Rumelhart. Forward models: Supervised learning with a distal teacher. *Cognitive Science*, 16(3):307–354, 1992.

[44] M. Katayama and M. Kawato. Virtual trajectory and stiffness ellipse during multijoint arm movement predicted by neural inverse models. *Biological Cybernetics*, 69:353–362, 1993.

[45] M. Kawato. Feedback-error-learning neural network for supervised learning. In R. Eckmiller, editor, *Advanced neural computers*, pages 365–372. North-Holland, Amsterdam, 1990.

[46] M. Kawato. Cerebellum and motor control. In M. A. Arbib, editor, *The handbook of brain theory and neural networks*, pages 172–178. MIT Press, Cambridge, MA, USA, 1998.

[47] M. Kawato. Internal models for motor control and trajectory planning. *Current Opinion in Neurobiology*, 9(6):718 – 727, 1999.

[48] M. Kawato. Cerebellum: Models. In L. R. Squire, editor, *Encyclopedia of Neuroscience*, pages 757 – 767. Academic Press, Oxford, 2009.

[49] M. Kawato and H. Gomi. The cerebellum and VOR/OKR learning models. *Trends in Neurosciences*, 15(11):445 – 453, 1992.

[50] M. Kawato and H. Gomi. A computational model of four regions of the cerebellum based on feedback-error learning. *Biological Cybernetics*, 68:95–103, 1992.

[51] A. M. Krylow, T. G. Sandercock, and W. Z. Rymer. The handbook of brain theory and neural networks. chapter Muscle models, pages 609–612. MIT Press, Cambridge, MA, USA, 1998.

[52] L. Lonini, L. Dipietro, L. Zollo, E. Guglielmelli, and H. I. Krebs. An internal model for acquisition and retention of motor learning during arm reaching. *Neural Comput.*, 21:2009–2027, July 2009.

[53] R. C. Miall. The handbook of brain theory and neural networks. chapter Motor control, biological and theoretical, pages 597–600. MIT Press, Cambridge, MA, USA, 1998.

[54] F. Mussa-Ivaldi, N. Hogan, and E. Bizzi. Neural, mechanical, and geometric factors subserving arm posture in humans. *The Journal of Neuroscience*, 5(10):2732–2743, 1985.

[55] F. A. Mussa-Ivaldi. Modular features of motor control and learning. *Current Opinion in Neurobiology*, 9(6):713 – 717, 1999.

[56] T. Nakayama and H. Kimura. Trajectory tracking control of robot arm by using computational models of spinal cord and cerebellum. *Syst. Comput. Japan*, 35:1–13, October 2004.

[57] K. Narendra and J. Balakrishnan. Adaptive control using multiple models. *Automatic Control, IEEE Transactions on*, 42(2):171 –187, feb 1997.

[58] R. Osu and H. Gomi. Multijoint muscle regulation mechanisms examined by measured human arm stiffness and EMG signals. *Journal of Neurophysiology*, 81(4):1458–1468, 1999.

[59] N. Özkaya, M. Nordin, and D. Leger. *Fundamentals of biomechanics: equilibrium, motion, and deformation*. Springer, 1999.

[60] J. Porrill, P. Dean, and J. V. Stone. Recurrent cerebellar architecture solves the motor-error problem. *Proceedings of the Royal Society of London. Series B: Biological Sciences*, 271(1541):789–796, 2004.

[61] D. Purves, G. J. Augustine, D. Fitzpatrick, L. C. Katz, A. S. Lamantia, J. O. Mcnamara, and M. S. Williams, editors. *Neuroscience*. Sinauer Associates, Inc., 3rd edition, 2004.

[62] R. M. Sanner and M. Kosha. A mathematical model of the adaptive control of human arm motions. *Biological Cybernetics*, 80(5):369, 1999.

[63] R. M. Sanner and J.-J. E. Slotine. Stable adaptive control of robot manipulators using "neuralt't' networks. *Neural Comput.*, 7:753–790, July 1995.

[64] N. Schweighofer, M. A. Arbib, and M. Kawato. Role of the cerebellum in reaching movements in humans. I. Distributed inverse dynamics control. *European Journal of Neuroscience*, 10(1), 1998.

[65] N. Schweighofer, J. Wolpert, Spoelstra, M. A. Arbib, and M. Kawato. Role of the cerebellum in reaching movements in humans. II. A neural model of the intermediate cerebellum. *European Journal of Neuroscience*, 10:95–105, 1998.

[66] R. Shadmehr. The handbook of brain theory and neural networks. chapter Equilibrium point hypothesis, pages 370–372. MIT Press, Cambridge, MA, USA, 1998.

[67] R. Shadmehr and O. A. Mussa-ivaldi. Adaptive representation of dynamics during learning of a motor task. *Journal of Neuroscience*, 14:3208–3224, 1994.

[68] R. Shadmehr and S. P. Wise. *The Computational Neurobiology of Reaching and Pointing : A Foundation for Motor Learning (Computational Neuroscience)*. The MIT Press, Jan. 2005.

[69] J.-J. Slotine and L. Weiping. Adaptive manipulator control: A case study. *Automatic Control, IEEE Transactions on*, 33(11):995 –1003, nov 1988.

[70] J.-J. E. Slotine and W. Li. On the adaptive control of robot manipulators. *Int. J. Rob. Res.*, 6:49–59, September 1987.

[71] J. Spoelstra, M. A. Arbib, and N. Schweighofer. Cerebellar control of a simulated biomimetic manipulator for fast movements. In P. van der Smagt and D. Bullock, editors, *Extended abstracts of the NIPS*97 Workshop - Can Artificial Cerebellar Models Compete to Control Robots?*, pages 28–32, 1997.

[72] J. Spoelstra, N. Schweighofer, and M. A. Arbib. Cerebellar learning of accurate predictive control for fast-reaching movements. *Biological Cybernetics*, 82(4):321, 2000.

[73] N. Sugimoto, J. Morimoto, S.-H. Hyon, and M. Kawato. eMOSAIC model for humanoid robot control. In *Proceedings of the 11th international conference on Simulation of adaptive behavior: from animals to animats*, SAB'10, pages 447–457, Berlin, Heidelberg, 2010. Springer-Verlag.

[74] E. Todorov and M. I. Jordan. Smoothness maximization along a predefined path accurately predicts the speed profiles of complex arm movements. *Journal of Neurophysiology*, 80(2):696–714, 1998.

[75] G. E. Uhlenbeck and L. S. Ornstein. On the Theory of the Brownian Motion. *Physical Review Online Archive (Prola)*, 36(5):823–841, Sept. 1930.

[76] S. Ushida and H. Kimura. Adaptive control of nonlinear system with time delay based on the feedback error learning method. In *SICE 2002. Proceedings of the 41st SICE Annual Conference*, volume 4, pages 2567 – 2572, aug. 2002.

[77] P. van der Smagt. Benchmarking cerebellar control. *Robotics and Autonomous Systems*, 23(3):237–251, 2000.

[78] S. Vijayakumar, A. D'Souza, and S. Schaal. Incremental online learning in high dimensions. *Neural Computation*, 17(12):2602 – 2634, 2005.

[79] D. M. Wolpert and M. Kawato. Multiple paired forward and inverse models for motor control. *Neural Networks*, 11(7-8):1317 – 1329, 1998.

[80] D. M. Wolpert, R. C. Miall, and M. Kawato. Internal models in the cerebellum. *Trends in Cognitive Sciences*, 2(9):338 – 347, 1998.

[81] K. Yamamoto, Y. Kobayashi, A. Takemura, K. Kawano, and M. Kawato. Computational Studies on Acquisition and Adaptation of Ocular Following Responses Based on Cerebellar Synaptic Plasticity. *J Neurophysiol*, 87(3):1554–1571, 2002.

Appendix A

Diagrams

1. FEL controller in the joint space with delay
2. FEL controller with separated adjuster signal and feedback controller including inverse and forward kinematics
3. Adaptive Controller based on Slotines's scheme [69]
4. Function based MOSAIC structure with FEL as the controller
5. ORF-MOSAIC with 4×4 modules and 7 parameters

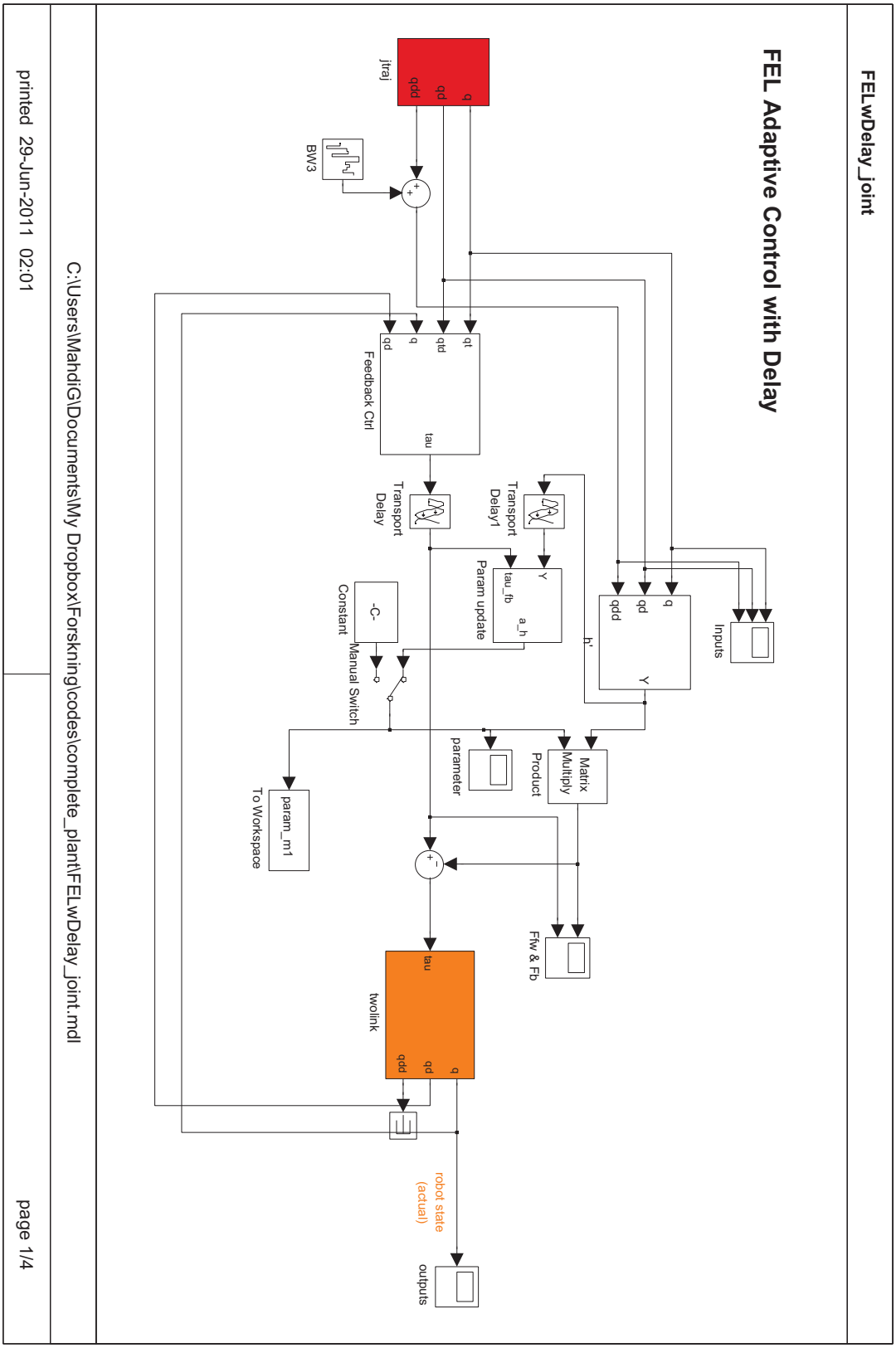
FELwDelay_joint
FEL Adaptive Control with Delay
jtraj
qdd
qd
q
BW3
Feedback Ctrl
qd
q
qtd
qt
tau
Transport Delay
Transport Delay1
Param update
tau_fb
a_h
Y
h'
Inputs
qdd
qd
q
Y
Constant
-C-
Manual Switch
parameter
Product
Matrix Multiply
To Workspace
param_m1
Ffw & Fb
twolink
tau
qdd
qd
q
robot state (actual)
outputs
C:\Users\MahdiG\Documents\My Dropbox\Forskning\codes\complete_plant\FELwDelay_joint.mdl
printed 29-Jun-2011 02:01
page 1/4

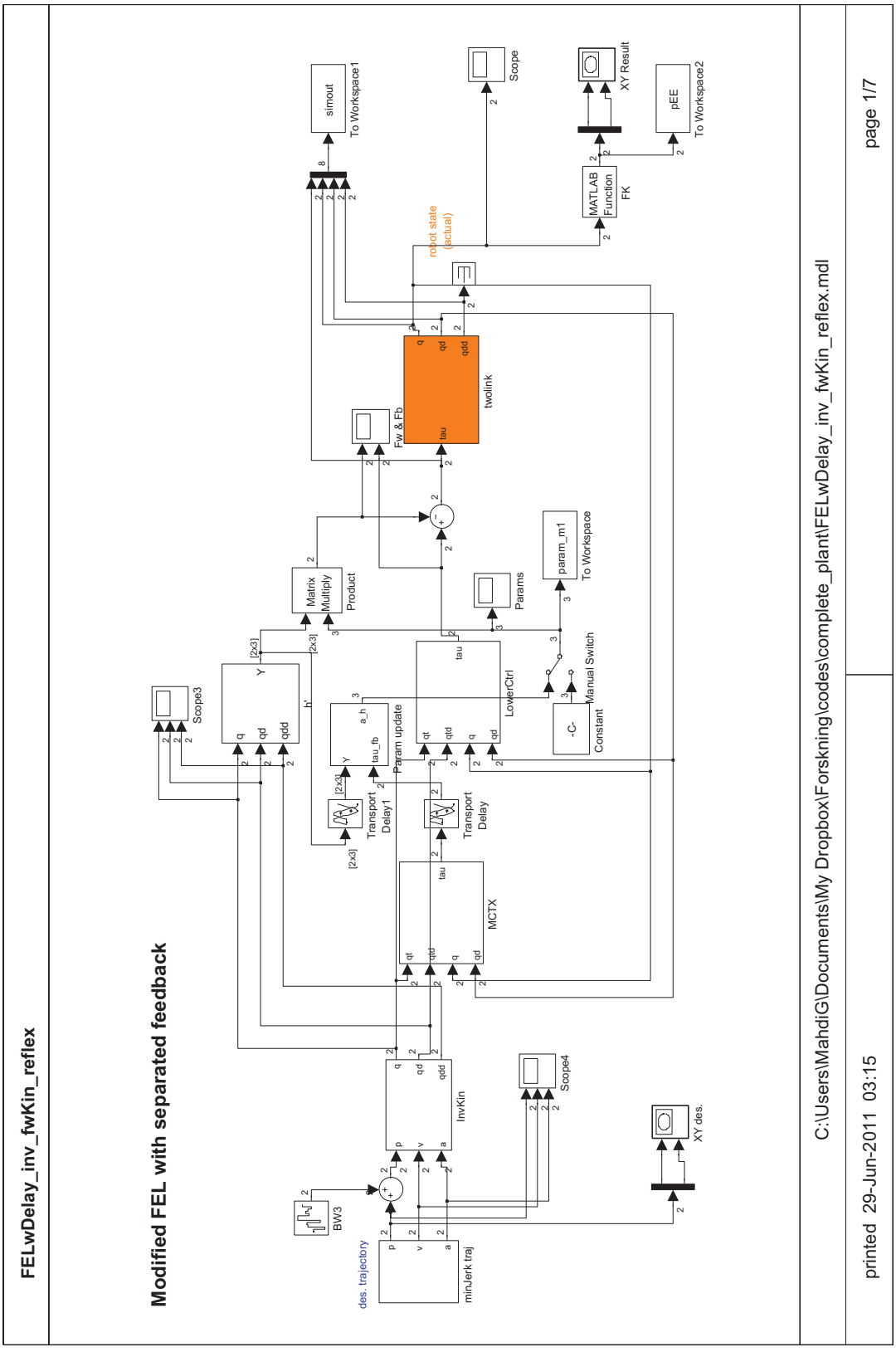
FELwDelay_inv_fwKin_reflex
Modified FEL with separated feedback
C:\Users\MahdiG\Documents\My Dropbox\Forskning\codes\complete_plant\FELwDelay_inv_fwKin_reflex.mdl
printed 29-Jun-2011 03:15
page 1/7
simout
To Workspace1
Scope
XY Result
pEE
To Workspace2
MATLAB Function
FK
robot state (actual)
twolink
Fw & Fb
Matrix Multiply
Product
Params
param_m1
To Workspace
Manual Switch
Constant
LowerCtrl
Param update
Transport Delay1
Transport Delay
MCTX
InvKin
Scope3
Scope4
XY des.
BW3
minJerk traj
des. trajectory

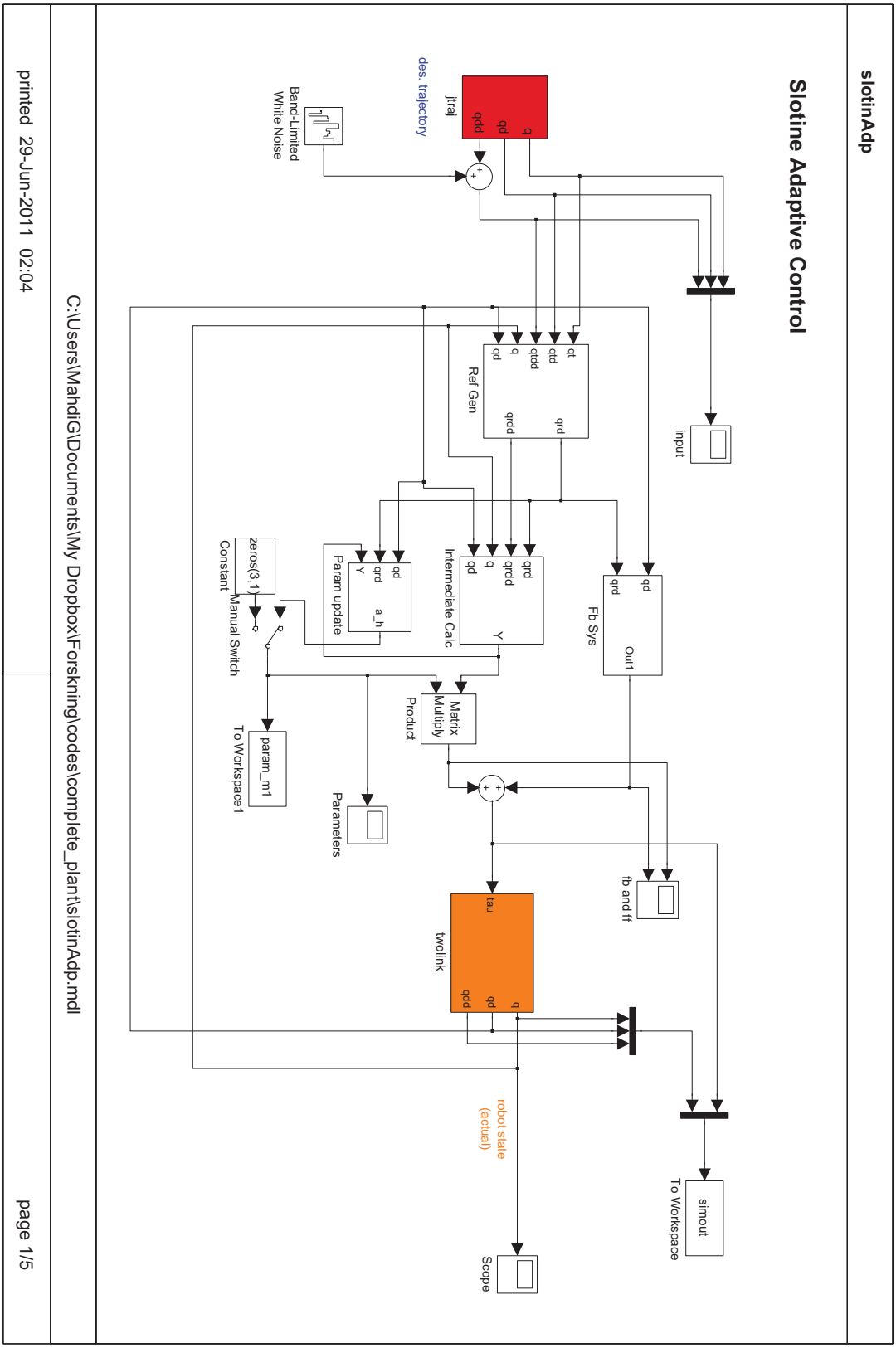
slotinAdp
Slotine Adaptive Control
C:\Users\MahdiG\Documents\My Dropbox\Forskning\codes\complete_plant\slotinAdp.mdl
printed 29-Jun-2011 02:04
page 1/5
jtraj
des. trajectory
Band-Limited White Noise
Ref Gen
input
Fb Sys
Out1
Intermediate Calc
Param update
zeros(3,1) Constant
Manual Switch
Matrix Multiply
Product
param_m1
To Workspace1
Parameters
fb and ff
twolink
tau
robot state (actual)
Scope
simout
To Workspace

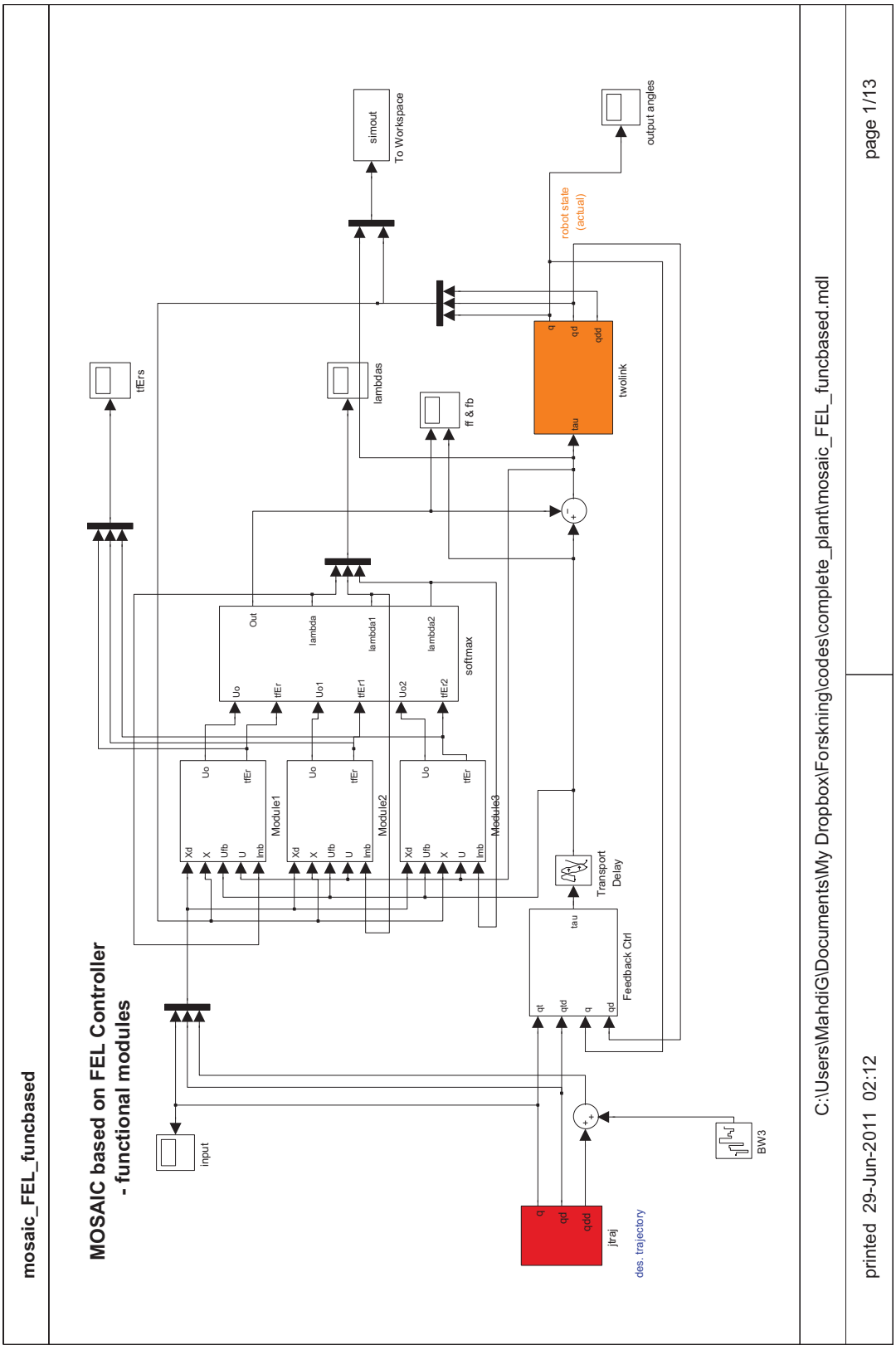
mosaic_FEL_funcbased
MOSAIC based on FEL Controller
- functional modules
C:\Users\MahdiG\Documents\My Dropbox\Forskning\codes\complete_plant\mosaic_FEL_funcbased.mdl
printed 29-Jun-2011 02:12
page 1/13
input
tfErs
simout
To Workspace
lambdas
ff & fb
output angles
robot state
(actual)
twolink
softmax
Module1
Module2
Module3
Transport
Delay
Feedback Ctrl
jtraj
des. trajectory
BW3

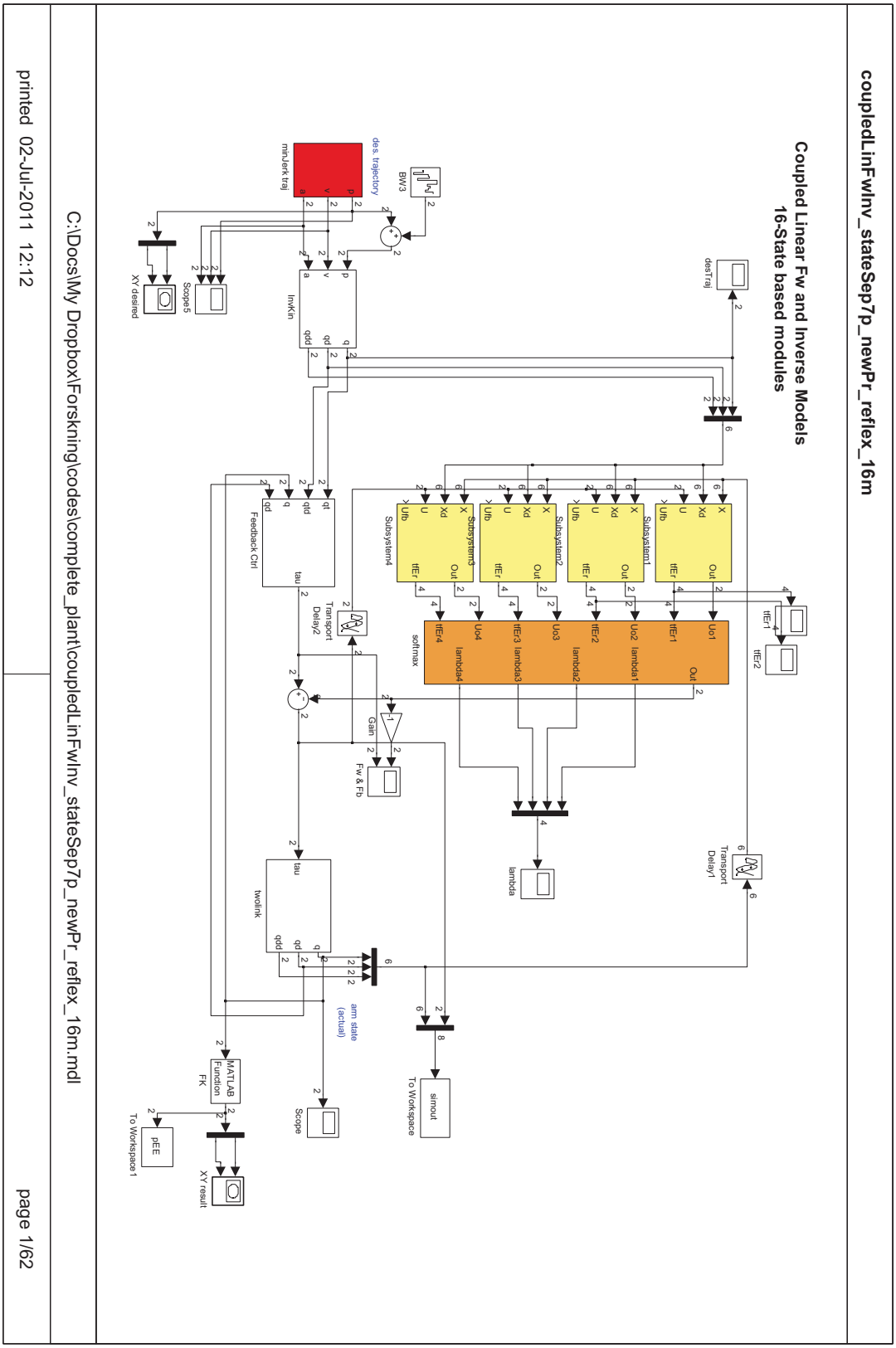
coupledLinFwInv_stateSep7p_newPr_reflex_16m
Coupled Linear Fw and Inverse Models
16-State based modules
C:\Docs\My Dropbox\Forskning\codes\complete_plant\coupledLinFwInv_stateSep7p_newPr_reflex_16m.mdl
printed 02-Jul-2011 12:12
page 1/62